PREPARATION AND CHARACTERIZATION OF HARD MAGNETIC NANOPARTICLES

by

DAREN LI

Presented to the Faculty of the Graduate School of

The University of Texas at Arlington in Partial Fulfillment

of the Requirements

for the Degree of

MASTER OF SCIENCE IN PHYSICS

THE UNIVERSITY OF TEXAS AT ARLINGTON

May 2006

ACKNOWLEDGEMENTS

I would like to sincerely express my gratitude to my advisor, Professor J. Ping Liu, for providing invaluable guidance and constant supports to my research and study. I highly appreciate Prof. Liu for introducing me to scientific research, giving me a chance to improve my research ability, and encouraging me to work in the field of nanotechnology. The present research work would have never been completed without Prof. Liu's proper guidance, regular supervision, and constant encouragement. His expertise in nanostructured magnetism along with his vision of nanotechnology has been the source of inspiration to me for further research in the field.

I would like to thank Professors Truman D. Black and Qiming Zhang for serving in my thesis committee. I am grateful for their careful and critical reading of my thesis and invaluable suggestions to make this thesis more scientifically solid. Their comments and suggestions will help to improve not only my research skill but also my insight in the future research.

I would also like to thank my colleagues Dr. Chuanbing Rong, Dr. Zhiqiang Jin, Dr. Baki Altuncevahir, Narayan Poudyal, Vikas Nandwana and Kevin Elkins for their important suggestions, cooperation and encouragement. Their contributions to my research work are greatly abundant and valuable. I am thankful to my other current and former colleagues, Dr. Yang Li, Dr. Girija S. Chaubey, Dr. YiPing Wang, Vamsi M. Chakka and Tejaswi Vedantam for their consistent helps and supports. Especially, I

appreciate Dr. Chuanbing Rong, Dr. Yang Li and Dr. YiPing Wang for spending their precious time reviewing my thesis and giving me valuable comments and suggestions.

I am thankful to our collaborator, Dr. Z.L. Wang in Georgia Institute of Technology for his cooperation in HRTEM analyses.

There can be no adequate acknowledgement for the love and encouragement that I have received from my parents, my wife, all other family members and my friends. Without their constant supports, all the works would have never been possible.

This work was supported by Defense Advanced Research Projects Agency (DARPA) through ARO under grant No. DAAD 19-03-1-0038 and Multidisciplinary University Research Initiative (MURI) under grant No. N00014-05-1-0479.

April 14, 2006

ABSTRACT

PREPARATION AND CHARACTERIZATION OF HARD MAGNETIC NANOPARTICLES

Publication No. _____

Daren Li, M. S.

The University of Texas at Arlington, 2006

Supervising Professor: J. Ping Liu

Hard-magnetic nanoparticles with uniform size distribution have attracted huge attention in the past several years because of their unique magnetic properties and potential for many applications such as high density recording media, exchange-coupled nanocomposite permanent magnets and biomedical applications. In this thesis, preparation and characterization of hard magnetic nanoparticles with different sizes are reported. Monodisperse FePt nanoparticles with face-centered cubic (fcc) structure were synthesized by chemical solution method and particle diameter was tuned from 2 to 15 nm by varying reaction conditions. Monodisperse hard-magnetic FePt nanoparticles

with ordered face-centered tetragonal (fct) structure were prepared by the salt-matrix annealing technique. Morphological, structural, and compositional characterizations of the nanoparticles were performed by Transmission Electron Microscopy (TEM), high resolution TEM (HRTEM), X-Ray Diffractometer (XRD), and Inductively Coupled Plasma-Optical Emission Spectroscopy (ICP-OES) analyses. Magnetic properties of nanoparticles of different sizes were studied by Alternating Gradiant Magnetometer (AGM), Superconducting Quantum Interference Device (SQUID) magnetometer and Vibrating Sample Magnetometer (VSM). It has been found that particle size has significant effect on the characteristics of the fct FePt nanoparticles, such as long-range ordering parameter, coercivity and Curie temperature.

TABLE OF CONTENTS

ACKNOWLEDGEMENTS ii

ABSTRACT iv

LIST OF ILLUSTRATIONS x

Chapter

1. INTRODUCTION OF MAGNETISM AND MAGNETIC MATERIALS .. 1

1.1 Introduction 1

1.2 Atomic Theory of Magnetism 2

1.3 Categories of Magnetism in Materials 3

1.3.1 Quantities and Units in Magnetism 6

1.3.2 Diamagnetism 7

1.3.3 Paramagnetism 7

1.3.4 Ferromagnetism 8

1.3.5 Antiferromagnetism and Ferrimagnetism 9

1.4 Ferromagnetic materials 10

1.4.1 Concepts 10

1.4.2 Soft Magnetic Materials 13

1.4.3 Hard Magnetic Materials 14

2. MAGNETIC NANOPARTICLES 18

2.1 Introduction 18

2.1.1 Single-Domain Particles 18

2.1.2 Superparamagnetism 19

2.2 Synthetic Techniques 21

2.3 FePt Nanoparticles 23

2.4 Soft Ferrite Nanoparticles 25

2.5 Applications of Magnetic Nanoparticles 27

3. CHEMICAL ORDERING AND MAGNETIC ORDERING IN NANOPARTICLES 32

3.1 Chemical Ordering 32

3.1.1 Introduction 32

3.1.2 Long-Range Ordering 32

3.1.3 Long-Range Ordering Parameter of FePt by X-ray Diffraction 37

3.1.4 Long-Range Ordering Parameter by Transmission Electron Microscope 39

3.1.5 Size-Dependent Chemical Ordering of FePt Nanoparticles 40

3.2 Magnetic Ordering 41

3.2.1 Introduction 41

3.2.2 Thermodynamic Properties at the Onset of Magnetic Ordering 42

3.2.3 Curie Temperatures of Nanoparticles 43

4. EXPERIMENTAL PROCEDURES AND EQUIPMENTS 45

4.1 Synthesis of FePt Nanoparticles 45

4.2 Salt-Matrix Annealing Technique 47

4.3 Characterization Techniques 49

4.3.1 X-Ray Diffraction (XRD) 49

4.3.2 Transmission Electron Microscope (TEM) 50

4.3.3 High-Resolution TEM (HRTEM) 52

4.3.4 Compositional Characterization 52

4.3.5 Magnetic Measurements 53

4.3.5.1 Sample Preparation for Magnetic Measurements 53

4.3.5.2 Alternating Gradient Magnetometer (AGM) 53

4.3.5.3 Superconducting Quantum Interference Device (SQUID) Magnetometer 54

4.3.5.4 Vibrating Sample Magnetometer (VSM) 55

5. RESULTS AND DISCUSSIONS 56

5.1 Long-Range Ordering of FePt Nanoparticles 56

5.1.1 Phase and Compositional Analysis 56

5.1.2 Long-Range Ordering Parameter 60

5.2 Morphology of fct FePt Nanoparticles 62

5.2.1 TEM Analyse 62

5.2.2 NaCl:FePt Ratio Effect 66

5.2.3 FePt Particle Size Effect 67

5.2.4 Annealing Condition Effect 68

5.3 Magnetic Properties of FePt Nanoparticles 69

5.4 Magnetic Ordering of FePt Nanoparticles 76

6. SUMMARY 81

Appendix

A. UNITS OF MAGNETIC PROPERTIES 84

B. CRYSTRAL STRUCTURE OF FERRITE 86

C. FePt PHASE DIAGRAM 88

D. RESEARCH ACOMPLISHMENTS 90

REFERENCES 94

BIOGRAPHICAL INFORMATION 110

LIST OF ILLUSTRATIONS

Figure		Page
1.1	The motions of an electron on the orbit about the nucleus in an atom	2
1.2	Ordering of magnetic moments in magnetic materials	4
1.3	Magnetization curves of diamagnetic, paramagnetic and antiferromagnetic materials	5
1.4	Magnetization curves of ferrimagnetic or ferromagentic materials	5
1.5	Magnetization curves of small particles with applied magnetic fields along its easy and hard directions	12
1.6	A full hysteresis loop. M_s is the saturation magnetization, M_r is the remanence magnetization and H_c is the coercivity	13
1.7	Hysteresis loops of typical hard and soft magnetic materils	14
1.8	A typical *B*-*H* loop of ferromagnetic materials	15
1.9	Evolution of $(BH)_{max}$ of permanent magnets in the 20th century	16
1.10	Hysteresis loops of soft, hard, and nanocomposite magnetic materials	17
2.1	(a) Coercivity dependence on particles diameter, (b) Typical magnetization curve of superparamagnetic materials	19
3.1	Ordered structures of (a) β-CuZn, (b) Cu_3Au and (c) CuAu	35
3.2	Atomic structures of (a) fcc and (b) fct phase FePt	37
4.1	Scheme for synthesis of FePt nanoparticles	46
4.2	The ball milling set-up for milling of NaCl powders	48
4.3	Büchi R-200 rotary evaporator	48

4.4 Bragg's law 50

4.5 Structure of the conventional TEM 52

5.1 XRD patterns of as-synthesized and annealed FePt nanoparticles with diameters of (a) 4 nm, (b) 6 nm, (c) 8 nm and (d) 15 nm 57

5.2 XRD pattern of 4 nm FePt nanoparticles annealed at 700 ^{o}C for 4, 6 and 8 hours 58

5.3 Selected area electron diffraction patterns of 2 nm FePt nanoparticles annealed at (a) 600 ^{o}C for 2 hours, (b) 700 ^{o}C for 4 hours and (c) 700 ^{o}C for 8 hours 59

5.4 (111) XRD peaks of 4 nm, 6 nm, 8 nm and 15 nm FePt nanoparticles annealed at 700 ^{o}C for 4 hours 60

5.5 Long-range ordering parameter vs. particle diameter for different annealing conditions 62

5.6 TEM images of salt-matrix annealed fct FePt nanoparticles annealed at 700 °C for 2 hours. (a) 15 nm with NaCl:FePt ratio of 100 : 1, (b) 8 nm with the ratio of 40 : 1, (c) 4 nm with the ratio of 40 : 1, (d) and (e) are the high resolution TEM images for (b) and (c), respectively 64

5.7 HRTEM image of an fct FePt nanoparticle annealed at 700 °C for 4 hours in salt-matrix, showing the polycrystalline morphology 65

5.8 TEM images of as-synthesized FePt nanoparticles (a) 2 nm, (b) 4 nm, (c) 6 nm, (d) 8 nm, (e) 15 nm and FePt nanoparticles (f) 2 nm annealed at 700^{o}C for 8 hours, (g) 4 nm, (h) 6 nm, (i) 8 nm, (j) 15 nm annealed at 700^{o}C for 4 hours 66

5.9 TEM images of 15 nm FePt nanoparticles (a) as-synthesized, and annealed in salt-matrix at 700 ^{o}C for 2 hours with NaCl:FePt ratios of (b) 4:1, (c) 40:1 and (d) 100:1 67

5.10 TEM images of 4 nm FePt nanoparticles annealed at (a) 700 ^{o}C for 2 hours with NaCl:FePt ratio of 40:1, (b) 700 ^{o}C for 4 hours with NaCl:FePt ratio of 100:1, (c) 700 ^{o}C for 8 hours with NaCl:FePt ratio of 100:1 and (d) 700 ^{o}C for 8 hours with NaCl:FePt ratio of 400:1 68

5.11 Hysteresis loops of 2 nm FePt nanoparticles annealed in salt-matrix in different conditions 70

5.12 Hysteresis loops of FePt nanoparticles with diameters of (a) 4 nm, (b) 6 nm, (c) 8 nm and (d) 15 nm annealed in different conditions 71

5.13 Coercivity vs. particle diameter under different annealing conditions 72

5.14 Coercivity vs. temperature for different particle sizes 72

5.15 Hystersis loops of 8 nm fct FePt nanoparticles aligned under 29 T magnetic field mixed in epoxy 73

5.16 Demagnetization curves measured at 10 K from the aligned and random 8 nm fct FePt nanoparticles in frozen alcohol 75

5.17 M-T loops of fct FePt nanoparticles with different sizes measured with and without salt-matrix 79

5.18 Curie temperature vs. particle diameter for samples measured with and without salt-matrix 80

5.19 ΔT_c vs. particle diameter, where ΔT_c is the difference in T_c between samples measured with and without salt-matrix 80

CHAPTER 1

INTRODUCTION OF MAGNETISM AND MAGNETIC MATERIALS

1.1 Introduction

The word “magnet” means “the stone from Magnesia” in Greek and Magnesia is the name of a Greek province where Greeks found the magnetite. Later on, huge and extensive efforts have been made on the study of magnetism and magnetic materials. In 1820, Oersted found that electric current could generate a magnetic field. The first electromagnet was then invented by Sturgeon five years later. Gauss, Maxwell and Faraday had significant contributions to theoretical magnetism. Curie and Weiss discovered the spontaneous magnetization and its relation with temperature. Bloch, Landau and Néel did systemic studies on magnetic domains. Magnetism is considered as an indispensable subject in science, engineering and technology, and magnetic materials are important components in wide applications of industries and medications. [1]

Magnetism is a very well known branch of physics and it is defined as a phenomenon in which an attractive or repulsive force is exerted by matters. If this phenomenon is caused by the movement of electrons from the change of electric field, it is classified as electromagnetism. On the other hand, if it is caused by the subatomic motion of electrons in substances, it is called permanent magnetism. [2-3] Therefore, in general, magnetic phenomena are caused by the motion of electrons.

1.2 Atomic Theory of Magnetism

All substances in nature are electronic, which means that all atoms are consist of positive and negative charges. The positive charges are called protons and the negative charges are called electrons. It is common knowledge that electric fields are caused spontaneously by electronic charges. However, as an integrally related aspect to electricity, magnetism is not caused by "magnetic" charges, which do not exist. Thus, the only source of magnetism is the relative motion of electronic charges. From the atomic point of view, there are two kinds of electronic motions, the orbital motion and the spin motion of electron. Figure 1.1 shows these two motions of electrons. The orbital motion is that an electron rotates around the nucleus and the spin motion is that an electron rotates around an axis that goes through its center. These two electron motions are the main source of most of the magnetic phenomena in substances. [1-6]

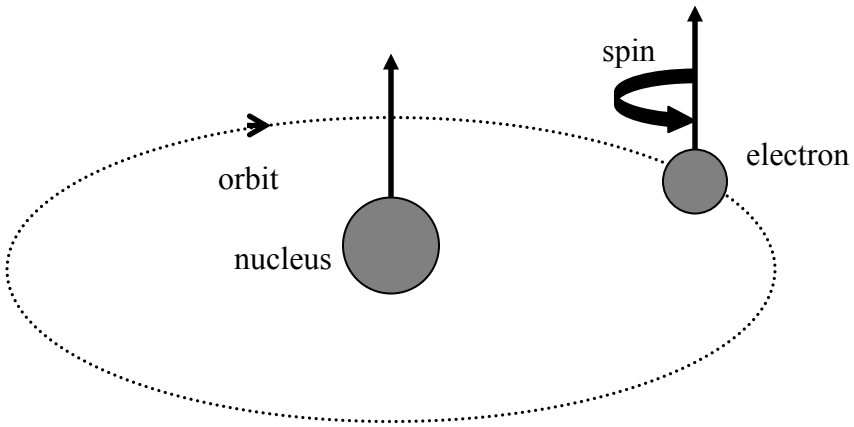

Figure 1.1 The motions of an electron on the orbit about the nucleus in an atom

1.3 Categories of Magnetism in Materials

When magnetic field is applied on the materials, different interactions of atomic moments with the field occur for different materials. According to these different interactions with a magnetic field, we can put materials into different categories. In nature, they are classified in three major categories: diamagnetism, paramagnetism and ferromagnetism. Another two categories of weakly attractive materials are ferrimagnetism and antiferromagnetism.

Figure 1.2 shows the ordering of magnetic moments in different magnetic materials. Except for classifying magnetic materials in how they react to an external magnetic field, we can also tell the difference from the magnetic ordering. The magnetic moments are oriented randomly in paramagnetic materials. Ferromagnetic materials have parallel-aligned magnetic moments. On the other hand, magnetic moments in antiferromagnetic and ferrimagnetic materials are both arranged in an antiparallel manner with the same and different magnitudes of moments, respectively.

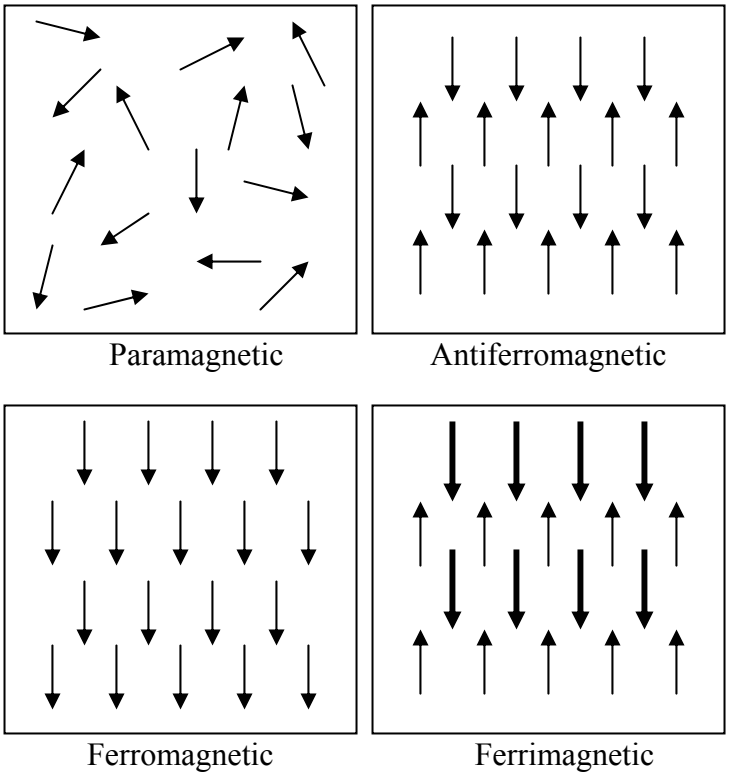

Figure 1.2 Ordering of magnetic moments in magnetic materials

The graphs of ***M*** or ***B*** versus ***H*** are called magnetization curves, which is another way to characterize the categories of magnetic materials. Figure 1.3 shows the magnetization curves of diamagnetic, paramagnetic and antiferromagnetic materials. All of these curves are linear with different signs of slopes, which give information about the susceptibility and permeability of the materials. Figure 1.4 shows the ***M-H*** curve of ferrimagnetic or ferromagnetic materials. The significant difference that distinguishes ferri- or ferromagnetic materials from others is that, firstly, a relatively larger magnetization is obtained when a small external magnetic field is applied. Secondly, the magnetization increases only very slightly when the applied field increases to a certain level, which is called saturation. From the curves, both susceptibility and permeability are

large and positive. Thirdly, the magnetization does not decrease to zero when the field decreases to zero, which indicates that ferri- and ferromagnetic materials have permanent magnetic moments.

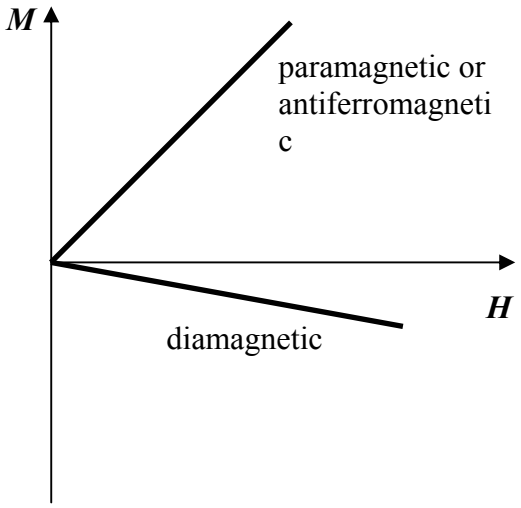

Figure 1.3 Magnetization curves of diamagnetic, paramagnetic and antiferromagnetic materials [6]

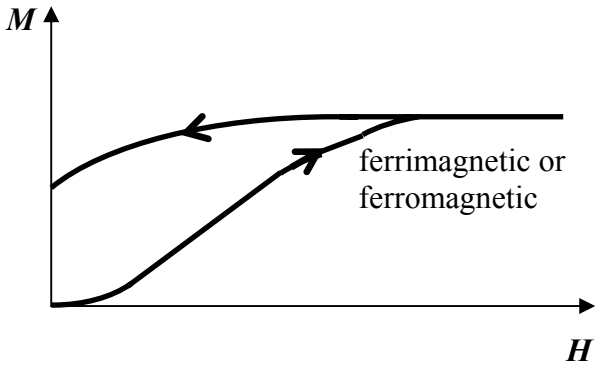

Figure 1.4 Magnetization curves of ferrimagnetic or ferromagentic materials [6]

1.3.1 Quantities and Units in Magnetism

Before we start the detail discussion about the different categories of magnetism in materials, let us get familiar with the common quantities and units in magnetism. A magnetic field can be created by a magnet or an electric current in the area around it. Magnetic field strength or intensity is usually described by $\boldsymbol{H}$ and the physical quantity that represents the effect of a magnet or current is the magnetic induction or magnetic flux density $\boldsymbol{B}$. In CGS units, the units of $\boldsymbol{B}$ and $\boldsymbol{H}$ are gauss (G) and oersted (Oe), respectively and the relation between $\boldsymbol{H}$ and $\boldsymbol{B}$ is:

$$\boldsymbol{B} = \boldsymbol{H} + 4\pi \boldsymbol{M} \tag{1.1}$$

where $\boldsymbol{M}$ is called magnetization or polarization which results from the two atomic motions mentioned above. Before defining $\boldsymbol{M}$, we need to know the definition of magnetic moment $\boldsymbol{m}$. Magnetic moment $\boldsymbol{m}$ is the moment of the torque exerted on the magnet when it is perpendicular to a uniform field of one Oersted. And magnetization $\boldsymbol{M}$ is the total magnetic moment $\boldsymbol{m}$ per unit volume and its unit is emu/cm^3.

The quantity that measures the efficiency that an applied field induces a magnetic dipole is called susceptibility,

$$\chi = \frac{\boldsymbol{M}}{\boldsymbol{H}} \tag{1.2}$$

And the ratio of $\boldsymbol{B}$ to $\boldsymbol{H}$ is called permeability, which indicates how permeable the material is to the magnetic field. A material with a larger amount of flux density in its interior has a higher permeability.

$$\mu = \frac{\boldsymbol{B}}{\boldsymbol{H}} \tag{1.3}$$

Using equation (1.1), (1.2) and (1.3), we can get,

$$\mu = 1 + 4\pi\chi \tag{1.4}$$

which only holds in CGS system of units.

1.3.2 Diamagnetism

Theoretically, diamagnetism results from the Lenz's law, which states that when an external magnetic field is applied on an electrical circuit, it induces in itself a current that is opposite in direction to the original current. This law also can be applied on electrons moving in an atomic orbit. When an increasing magnetic field is applied, the induced current decreases the orbital magnetic moment. Therefore, the differential susceptibility $\chi = \frac{dM}{dH}$ is negative. We call this phenomenon diamagnetism. [4-6] NaCl and CuO are the examples of diamagnetic materials.

1.3.3 Paramagnetism

Paramagnetic materials are those with non-zero magnetic moment on their atoms, ions or molecules. Thus, an applied magnetic field can align these moments to create a positive susceptibility. At the same time, diamagnetic phenomenon also occurs, but the atomic moments are much greater than the induced moments in magnitude. The inverse dependence of susceptibility on temperature in paramagnetism is known as Curie's law. [1-6]

$$\chi = \frac{\boldsymbol{M}}{\boldsymbol{H}} = \frac{C}{T} \tag{1.5}$$

where C is a constant. Many salts of transition elements and some of the metals such as aluminum are of paramagnetism. Ferromagnetic and antiferromagnetic materials above a critical temperature of magnetic ordering also show paramagnetic behavior.

1.3.4 Ferromagnetism

Ferromagnetic materials are characterized by a spontaneous parallel alignment of atomic magnetic moments, such as iron, nickel and gadolinium. This alignment disappears when temperature is above a critical temperature that is called Curie temperature. In ferromagnetic materials, there is a non-zero magnetic moment even in the absence of an external magnetic field. In 1906, Weiss for the first time described the phenomenon of ferromagnetism by his molecular field theory. [3-4] According to his theory, each of the atomic moments is interacting with each other magnetically. The net interaction of all the moments causes an effective magnetic field, which is proportional to the magnetization.

$$\boldsymbol{H}_E = \alpha \boldsymbol{M} \tag{1.6}$$

Then the total magnetic field comprising the external field is:

$$\boldsymbol{H}_{tot} = \boldsymbol{H} + \boldsymbol{H}_E = \boldsymbol{H} + \alpha \boldsymbol{M} \tag{1.7}$$

Substituting equation (1.7) in equation (1.5),

$$\boldsymbol{M} = \frac{C}{T}\left(\boldsymbol{H} + \alpha \boldsymbol{M}\right) \tag{1.8}$$

Using the definition of susceptibility $\chi = \dfrac{\boldsymbol{M}}{\boldsymbol{H}}$,

$$\chi = \frac{\boldsymbol{M}}{\boldsymbol{H}} = \frac{C}{T - \alpha C} = \frac{C}{T - T_c} \tag{1.9}$$

Equation (1.9) is called Curie-Weiss law with $T_c = \alpha C$ as the Curie temperature. It describes the temperature dependence of the susceptibility on temperature above T_c.

When $T = T_c$, the susceptibility χ diverges, which means a none-zero $\boldsymbol{M}$ exits even when the applied magnetic field $\boldsymbol{H}$ is zero. This none-zero $\boldsymbol{M}$ is called spontaneous magnetization. When $T > T_c$, there is no spontaneous magnetization without applied magnetic field. However, a non-zero magnetization appears again under the influence of an external magnetic field and the susceptibility behavior of a ferromagnetic matter is analogous to that of a paramagnetic one. [1, 4-5]

1.3.5 Antiferromagnetism and Ferrimagnetism

In an antiferromagnetic material, there are neighboring atomic moments which have exchange coupling. This effect results in an antiparallel orientation of moments, which is exactly the opposite of ferromagnetic materials. Because of this antiparallel alignment of moments, the magnetization is zero and the susceptibility is small and positive. At a temperature above a critical point, the susceptibility of antiferromagnetic materials follows a paramagnetic behavior. The examples of antiferromagnetism include FeO, and Fe_3Mn. [1-6]

Ferrimagnetic materials are similar to aniferromagnetic materials in which the coupling effect creates an antiparallel alignment of magnetic moments. However, differently from antiferromagnetic materials, the magnetic moments are not equal to each other so they do not cancel each other and a finite net moment exits, which is known as a spontaneous magnetization. Magnetites like FeO·(Fe2O3) and GdFe2 are of ferrimagnetism. [1-6]

1.4 Ferromagnetic materials

Ferromagnetic materials are of great value due to their property of permanent magnets. Understanding of some important concepts and the classification of ferromagnetic materials according to their characteristics is very helpful for better applications.

1.4.1 Concepts

Curie temperature (T_c) - It is a critical temperature at which the thermal energy overcomes the exchange interaction between magnetic movements and results in randomization. At a temperature lower than the Curie temperature, the magnetic moments are oriented in a parallel manner, which results in spontaneous magnetization characterizing the property of permanent magnets. Above the Curie temperature, this parallel orientation of magnetic moments disappears and the material shows a similar behavior as paramagnetism. When this happens, the material will lose all the spontaneous magnetization.

Magnetic domains - In theory, in a piece of ferromagnetic material below its Curie temperature, the exchange energy aligns all the atomic magnetic moments so that they act cooperatively to yield a macroscopic total magnetic moment. Nevertheless, this piece of ferromagnetic material usually has no magnetic moment with the absence of external magnetic field. In 1906, Weiss gave the solution to this puzzle. [3-4] He proposed that there are many small regions in the ferromagnetic materials, which have magnetic moments pointing to different directions. These small regions are called magnetic domains. By canceling out each other, the total magnetic moment remains

nearly zero. The boundaries between different domains are called domain walls, which are a result of competition of energies. [4-5]

Magnetic Anisostropy - Magnetic anisotropy means the dependence of the magnetic properties on the direction in which they are measured. [3-4, 6] Magnetic properties such as magnetization and hysteresis are affected by the magnitude and type of the magnetic anisotropy. The energy associated with the alignment of magnetization due to magnetic anisotropy is called anisotropy energy and given by:

$$E_a = K \sin^2 \theta \tag{1.10}$$

where θ is the angel between $\boldsymbol{M_s}$ and the easy axis and K is the anisotropy constant. There are two important categories of magnetic anisotropy, magnetocrystalline anisotropy and shape anisotropy.

Magnetocrystalline anisotropy is intrinsic to materials while all other types of anisotropy are induced by processing methods. In magnetocrystalline anisotropy, the magnetization tends to orient itself along a preferred crystallographic direction called the easy axis. The magnetocrystalline anisotropy energy can be defined as the energy difference between samples magnetized along easy and hard directions. One example of magnetocrystalline anisotropy like iron and nickel is shown in figure 1.5. The easy axis for iron and nickel is (100) and (111), respectively. The final spontaneous magnetization is the same for both easy and hard directions but the applied field needed to reach that value is obviously different in each direction.

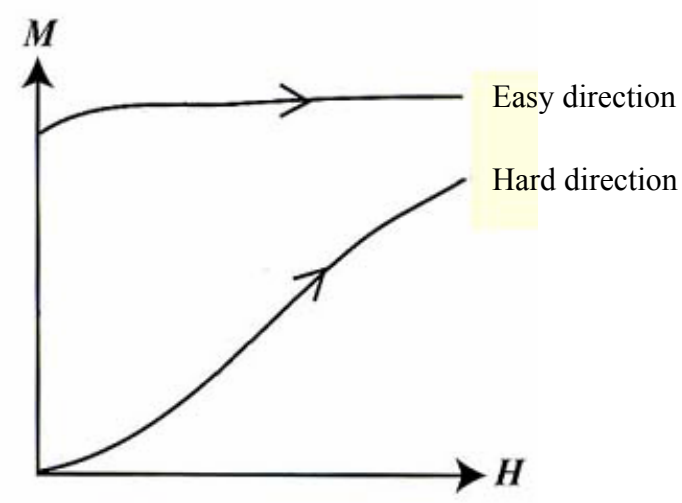

Figure 1.5 Magnetization curves of small particles with applied magnetic fields along its easy and hard directions

Although a polycrystalline sample without any preferred orientation in its grain does not have overall magnetocrystalline anisotropy, it will be easier to be magnetized along the long axis if the shape of sample is not spherical, which is known as shape anisotropy. The cause of shape anisotropy is that the demagnetizing field is less along the long axis direction because the induced poles at the surface are farther apart and the smaller applied field negates the demagnetizing field. The shape anisotropy can be as important as magnetocrystalline anisotropy. For example, a long rod of iron with M_s=1714 emu/cm^3 has a shape anisotropy constant K_s=1.85×10^7 erg/cm^3, which is much greater than many cases of magnetocrystalline anisotropy. [3-4]

Hysteresis - When a piece of ferromagnetic material is magnetized by an increasing applied magnetic field and then the field is decreased, the magnetization does not follow the initial magnetization curve obtained during the increase. In other words, it

is a phenomenon of irreversibility of magnetization curve and this phenomenon is called hysteresis. [4, 6] As described in figure 1.6, as the applied field $\boldsymbol{H}$ increases, magnetization approaches to a saturation value $\boldsymbol{M_s}$, which is called saturation magnetization. The magnetization does not go back to zero when the field decreases to zero. Instead, it remains a certain value of magnetization when the field is zero, which is called remanence $\boldsymbol{M_r}$. When the magnetic field is applied in a revered direction, magnetization reaches zero at a field magnitude called coercivity $\boldsymbol{H_c}$. Further increase of field in the reversed direction, the ***M*-*H*** curve follows the same behavior as the positive side. This ***M*-*H*** curve is then called the hysteresis loop.

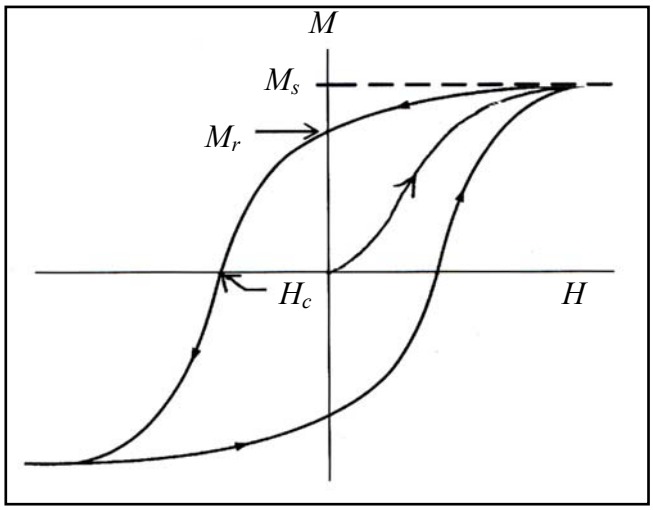

Figure 1.6 A full hysteresis loop. M_s is the saturation magnetization, M_r is the remanence magnetization and H_c is the coercivity

1.4.2 Soft Magnetic Materials

Ferromagnetic materials are generally divided into two categories, soft magnetic and hard magnetic materials, according to their hysteresis properties. Soft magnetic materials are those that can be magnetized and demagnetized very easily under low

strength of external magnetic field. There is low magnetization left after the field is removed. Therefore, relatively, soft magnetic materials have low coercivity, typically less than 10 Oe, high saturation magnetization M_s but low remanence M_r, as shown in figure 1.7. Materials such as iron, silicon iron, aluminum iron, etc., are common soft magnetic materials. They are widely used in the magnetic cores of transformers, motors, inductors and generators.

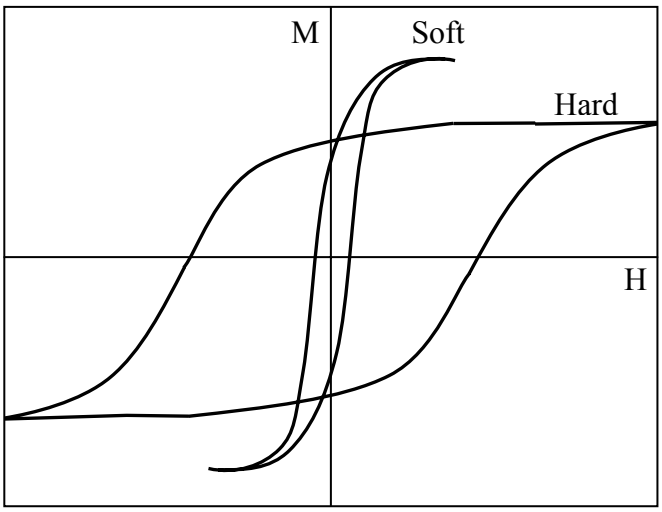

Figure 1.7 Hysteresis loops of typical hard and soft magnetic materials

1.4.3 Hard Magnetic Materials

In the *B-H* loop shown in figure 1.8, the maximum product value of *B* and *H* is called the maximum energy product $(BH)_{max}$, which is a parameter to demonstrate the maximum work that can be done by the magnet. Therefore, $(BH)_{max}$ is the figure of merits for permanent magnetic materials. Large coercivity H_c and saturation magnetization M_s result in large $(BH)_{max}$. However, for materials with sufficiently high H_c values ($H_c > 2\pi M_s$), the theoretical limit of the energy product is, [7]

$$(BH)_{\max} \le (2\pi M_s)^2 \tag{1.11}$$

From figure 1.8, we can see the $(BH)_{max}$ also depends on the shape of the hysteresis loop. Hysteresis loops with higher squareness result in higher maximum energy products.

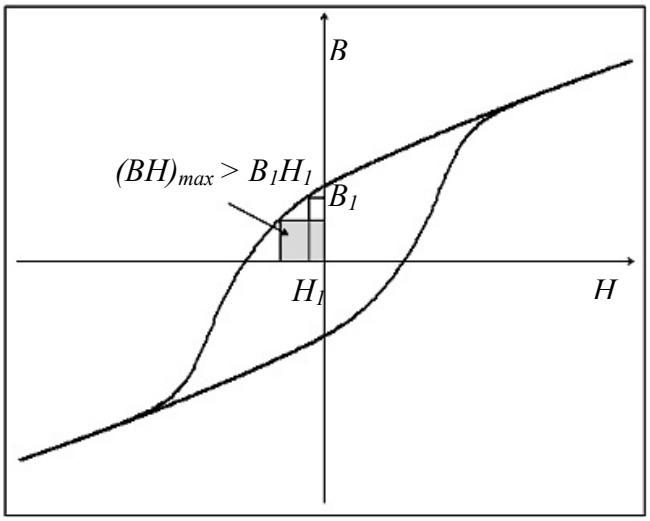

Figure 1.8 A typical *B*-*H* loop of ferromagnetic materials

The term "hard" means that this kind of materials is more difficult to be demagnetized. Therefore, it requires higher magnetic field to be demagnetized to zero, which indicates that the coercivity is higher. In fact, the relatively high coercivity, which is usually larger than 1000 Oe, is the evidence of hard magnetic materials, as shown in figure 1.7. Also, the remaining magnetization is relatively large after removal of the magnetizing field, which means that the hard magnetic materials have higher remanence M_r. Because of this ability to store magnetization in the absence of field, hard magnetic materials are also known as permanent magnetic materials. The most well known hard magnetic materials are cobalt-rare earth alloys ($SmCo_5$ and Sm_2Co_{17}), neodymium-iron-

boron ($Nd_2Fe_{14}B$), iron-platinum (FePt), cobalt-platinum (CoPt), hard ferrites ($SrO\text{-}Fe_2O_3$ or $BaO\text{-}6Fe_2O_3$) and Alnicos.

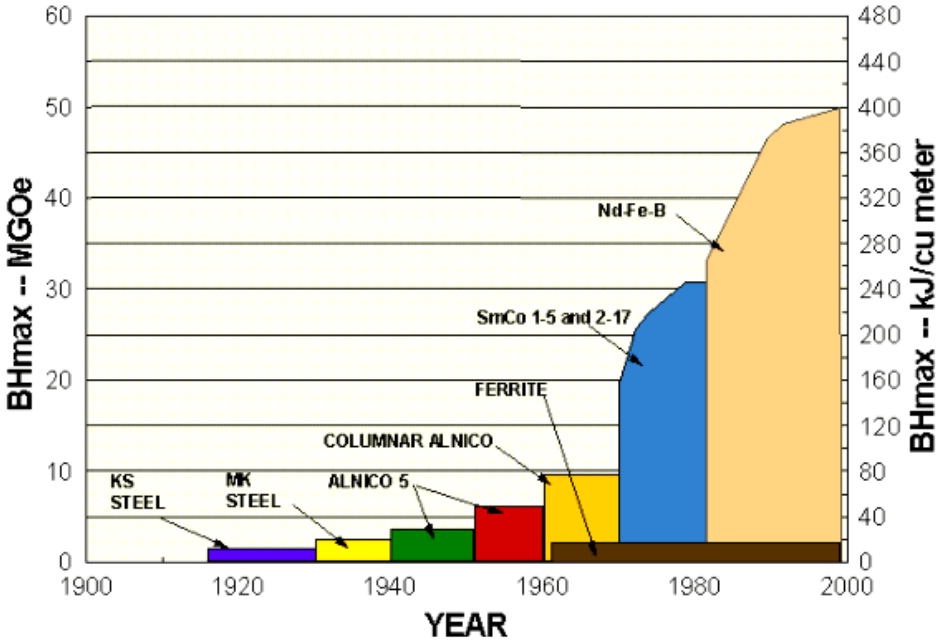

Figure 1.9 Evolution of $(BH)_{max}$ of permanent magnets in the 20th century

The performance of a permanent magnetic material is specified by the value of $(BH)_{max}$. As the hard magnetic materials are being developed, $(BH)_{max}$ has experienced a huge increase in the past one hundred years, as shown in figure 1.9. [8] Driven by the theoretical limit of maximal energy product described by equation (1.11), huge efforts have been put into developing new hard magnetic materials with high anisotropy and magnetization. However, these new hard-magnetic compounds such as $SmCo_5$, Sm_2Co_{17} and $Nd_2Fe_{14}B$ have magnetization values significantly lower than those of traditional soft magnetic materials, which results in lower theoretical limit of maximal energy product ($4\pi M_s$), compared to Co, Fe or $Fe_{65}Co_{35}$ with the $4\pi M_s$ values of 18, 21, and 24 kG,

respectively [7]. Researchers began to realize that it is difficult for magnetic materials with only single phase to reach another stage of energy product. In 1991, Kneller and Hawig proposed an alternative approach to enhance the energy product by making a nanocomposite of exchange-coupled hard and soft magnetic phases. [9] The hard phase provides the high magnetic anisotropy and stabilizes the exchange-coupled soft phase against demagnetization and the soft phase provides the high magnetization to enlarge the maximal energy product $(BH)_{max}$, as shown in Figure 1.10.

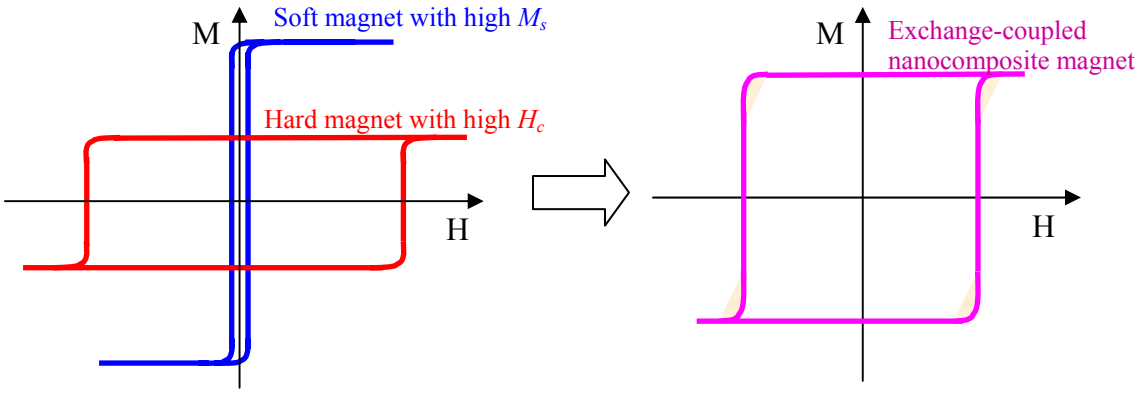

Figure 1.10 Hysteresis loops of soft, hard, and nanocomposite magnetic materials

Coehoorn and colleagues for the first time observed the exchange-coupled nanocomposite in a melt-spun $Nd_{4.5}Fe_{77}B_{18.5}$ sample that was annealed with the presence of the Fe_3B phase. [10] Skomski and Coey did systemic theoretical study of exchange coupled films and predicted that energy product as high as 120 MGOe might be reachable by the exchange coupling in oriented nanostructured magnetic materials. [11, 12]

CHAPTER 2

MAGNETIC NANOPARTICLES

2.1 Introduction

Nanoparticles are typically defined as solid substances less than 100 nm in all three dimensions. The productions and applications of uniform nano-scaled particles have been rapidly developed in the past two decades due to the fact that small size and high surface-to-volume ratio of nanoparticles provide unique physical and chemical properties. [15, 44, 51] Magnetic nanoparticles are of special interest because of their unique magnetic properties due to their nano size (<100 nm) and they have great potential in many technological applications. [40]

2.1.1 Single-Domain Particles

The magnetostatic energy of a material could be decreased by restructuring it into domains. [3-4] Because it needs energy to complete the formation of domains, in large volume of particle there would be a minimum domain size below which the energy needed for domain formation exceeds the benefits from decreasing the magnetostatic energy. This means a single particle with size comparable to the minimum domain size will not break into domains and remains single domain. [3-4]

The magnetization of a single-domain particle lies along the easy axis direction in the absence of applied magnetic field. When a field is applied opposite to the direction of the magnetization, the magnetic moments rotate through the hard direction to a new easy

direction. There is no domain structure change with this magnetization switching. It is always more difficult to overcome the anisotropy force that holds the magnetization in the easy direction to rotate the magnetization than to move a domain wall, thus, single-domain particles have a larger coercivity than multi-domain materials, as shown in figure 2.1 (a).

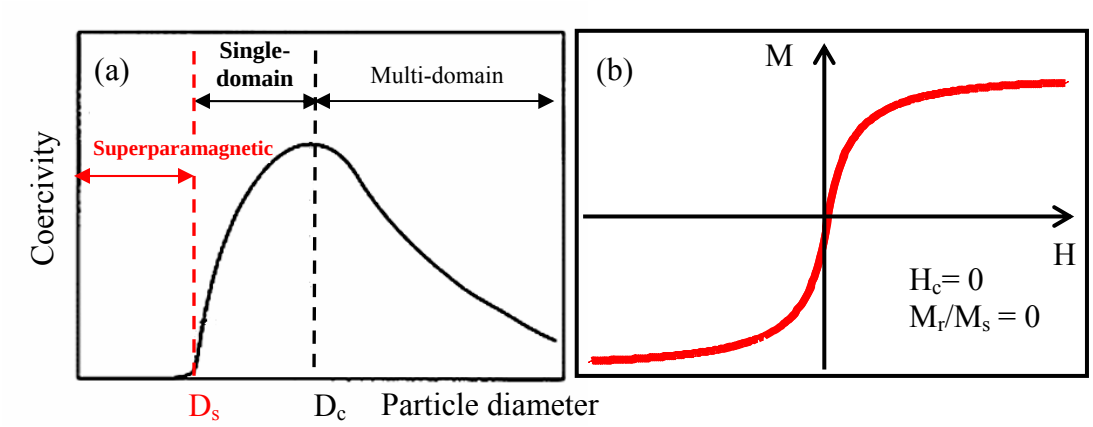

Figure 2.1 (a) Coercivity dependence on particles diameter, (b) Typical magnetization curve of superparamagnetic materials

2.1.2 Superparamagnetism

The phenomenon of superparamagnetism is observed in small single-domain particles and it occurs when the materials are composed of very small particles (usually below10 nm). [3-4] The energy required to change the direction of magnetization of a crystallite is called the crystalline anisotropy energy, which depends on both the material properties and the particle size, as described in the following equation,

$$E_a = K_\mu V \tag{2.1}$$

where K_μ is the anisotropy energy density and V is the magnetic switching volume of the crystallite. As the crystallite size V decreases, so does the crystalline anisotropy energy.

When the crystallite size reaches below a critical limit, the thermal energy is sufficient to overcome the coupling interactions between neighboring atoms even though the temperature is below the Curie or Neel temperature, which leads to the change in direction of magnetization of the entire crystallite. The resulting fluctuation of the magnetization direction causes the magnetic field to average to zero. The material behaves in a manner similar to paramagnetism, except that the magnetic moments of the entire crystallite tend to align under the magnetic field instead of each individual atom being independently influenced by an external magnetic field. A typical magnetization curve measured from superparamagnetic materials is shown in figure 2.1 (b).

This superparamagnetic size limit can be estimated by the Neel relaxation time equation given below, [123]

$$t_{rel} = \tau_o \exp\left(\frac{K_\mu V}{k_B T}\right) \tag{2.2}$$

where τ_o is the relaxation time factor of the order of 10^{-9} seconds and $k_B T$ is the thermal energy with the Boltzmann constant k_B. When the magnetic measurement time $t_{meas} < t_{rel}$, the sample belongs to ferromagnetism. And when $t_{meas} > t_{rel}$, it belongs to superparamagnetism. Therefore, the ratio of crystalline anisotropy energy $K_\mu V$ to the thermal energy $k_B T$ should satisfy the condition below for the superparamagnetic size limit,

$$\frac{K_\mu V}{k_B T} \geq ln\left(\frac{t_{meas}}{\tau_o}\right) \tag{2.3}$$

In the case of high-K_μ magnetic mateials such as FePt, $SmCo_5$ and CoPt, etc., in order to maintain the thermal stability of the sigle-domain nanoparticles, this ratio should satisfy, [118-120]

$$\frac{K_\mu V}{k_B T} \geq 60 \tag{2.4}$$

Therefore, we can estimate the superparamagnetic size limit D_s by assuming the cubic shape of grains, [13]

$$D_s = \left(\frac{60 \cdot k_B T}{K_\mu} \right)^{\frac{1}{3}} \tag{2.5}$$

As for FePt nanoparticles, taking K_μ=6.6~10×10^7 erg/cm^3, T=300 K and k_BT=3.77×10^{-14} erg, the superparamagnetic size limit D_s is 2.8~3 nm at room temperature. [13, 121, 122] This theoretical superparamagnetic size limit also predicts that FePt nanoparticles below a critical size limit can not convert to hard magntic phase. [13] This transition size limit has been proved to be well matched with the range of the superparamagnetic size limit, theoretically and experimentally. [109-111, 113]

2.2 Synthetic Techniques

The preparations of monodisperse magnetic nanoparticles can be divided into "bottom-up" or "top-down" methods. In a "bottom-up" approach, small building blocks such as atoms and clusters are assembled to form nanoparticles. Examples of this approach include chemical synthesis, laser-induced assembly and colloidal aggregation. [55, 59-64, 68, 78-82] In the top-down approach, large objects are broken down to finer

particles such as mechanical milling. [83, 84] Various synthetic strategies for preparation of magnetic nanoparticles have been investigated, including chemical co-precipitation [51, 59], sonochemical reactions [81, 85], sol-gel [86, 87], microwave heating [88, 89], mechanochemical [50, 90], micelle microemulsion [55, 61, 62, 79, 80, 91], hydrothermal [55, 92], and ball milling [83, 84]. Compared to other methods, chemical synthesis has often been found the best method for the production of high- quality magnetic nanoparticles.

The chemical synthesis of nanoparticles in a solution occurs by chemical reactions forming stable nuclei with subsequent particle growth. [44, 50] Upon the addition of precipitating, reducing, or oxidizing reagents to the solution containing the reactants, chemical reactions occur and solution becomes supersaturated with products. The thermodynamics equilibrium state of the system is restored by condensation of nuclei of the reaction product. Kinetic factors compete with the thermodynamics of the system in a growth process. The kinetic factors such as reaction rates, transport rates of reactants, accommodation, removal, and redistribution of matter compete with influence of thermodynamics in particles growth. The particle morphology is influenced by factors such as supersaturation, nucleation and growth rate, colloidal stability, recrystallization and aging process. When the nuclei are formed nearly at the same time in a supersaturated solution, subsequent growth of these nuclei results in the formation of particles with a very narrow size distribution. To maintain a narrow size distribution, it is very important to prevent agglomeration, Ostwald ripening, or continued nuclei formation.

Nanoparticles possess large surface areas and often form agglomerates as a result of attractive van der Waals forces and the tendency of the system to minimize the total surface or interfacial energy. Agglomeration of particles can occur during any of the following stages: synthesis, drying, handling, and processing. In many applications and processing where dispersed particles or stabilized dispersions are required, undesirable agglomeration in each synthesis and processing step must be prevented. Surfactants are any substance that lowers the surface or interfacial tension of the medium in which it is dissolved. Surfactants are used during nanoparticles synthesis in order to reduce particle interaction through an increase in repulsive forces. They are used to control particle size and distribution in most chemical synthesis routes.

2.3 FePt Nanoparticles

FePt nanoparticles draw great attention from nanomagnetism researchers because it is the only available type of hard magnetic nanoparticles with high magnetocrystalline anisotropy ($6.6\sim10.0\times10^7$ erg/cm^3). [13] They are the most promising candidate for ultrahigh-density magnetic recording media [14], high-energy-product permanent magnets [15] and sensors and drug carriers in biomedical technology [16]. There are different approaches to produce FePt nanoparticles, such as mechanical ball milling [34] and sputtering deposition [35]. However, the magnetic properties and particle size distribution are not qualified for the applications mentioned above. In the year of 2000, Sun and co-workers reported their breakthrough in chemical synthesis of FePt nanoparticles [14]. These chemically synthesized FePt nanoparticles are monodisperse with very uniform size distribution. Since this milestone was built, the synthesis of

monodisperse FePt nanoparticles with size ranging from 2 to 15 nm have been achieved successfully [14, 17-19, 36]. However, as-synthesized FePt nanoparticles are of face-centered cubic (fcc) phase that does not provide any magnetocrystalline anisotropy required by the applications mentioned above. In order to solve this problem, heat treatment at a temperature higher than 500^{o}C must be performed to transfer fcc phase to face-centered tetragonal phase (fct) with high magnetocrystalline anisotropy. Undesirably, coalescence and sintering of nanoparticles also occur at these temperatures because surfactants coating on the nanoparticles decomposes at around 400^{o}C. [30] This coalescence and sintering phenomenon makes the direct applications of monodisperse hard magnetic nanoparticles impossible.

Extensive efforts have been made to obtain monodisperse fct FePt particles. One of the approaches is to lower the onset temperature for the fcc-to-fct phase transition. By doping mental elements such as Ag, Au and Cu in the FePt phase, the onset temperature of the fct phase was lowered to 400°C. [20-25] Direct synthesis of the fct structured FePt nanoparticles by the polyol process using high-boiling-point solvents is another major approach. [26-29] In this approach, higher synthetic temperatures are applied, which allows partial formation of the fct phase. Recently, the method of protecting FePt nanoparticles from sintering during heat treatments by chemically stable coating materials has been developed. Immiscible silica matrix [30], and polyethyleneimine linker molecules [31] are one of these coating materials. FePt nanoparticle arrays with these coating were annealed at temperatures higher than 700 ^{o}C without sintering. However, these two approaches are only suitable for monolayers of separated

nanoparticles on substrates. The technique of coating monodisperse FePt nanoparticles with silicon oxide appeared later on, which allows the heat treatment temperatures as high as 900 ^{o}C without sintering. [37, 38] Nevertheless, the addition of chemically stable impurities from the coating is the huge holdback of the hard magnetic nanoparticles applications. Other approaches to obtain monodisperse fct nanoparticles include rapid thermal annealing [32] and pulse laser annealing [33]. So far, all these reported approaches have been only successful in producing partially transformed fct FePt nanoparticles and high coercivities needed for the applications mentioned above have not been developed. On the other hand, coating techniques brought in the inexpungible impurities in spite of completing the fct phase transition. Therefore, in order to make the applications of hard magnetic nanoparticles realized, it is highly desirable to find processing techniques to produce completely transformed fct FePt nanoparticles. In 2005, Liu's group [70] made a great break-though by successfully preparing monodisperse fct FePt nanoparticles with high coercivity and without remaining any nonmagnetic impurities, which started the new chapter of the direct applications of hard magnetic nanoparticles with high magnetic anisotropy.

2.4 Soft Ferrite Nanoparticles

There is an increasing interest in magnetic ferrite nanoparticles in recent years because of their broad applications in different technological fields including permanent magnets, magnetic fluids, magnetic drug delivery, and high-density recording media. [15, 39-54] The cubic MFe_2O_4 or $MO{\cdot}Fe_2O_3$ (M = Fe, Co) is a common type of magnetic ferrite that has a cubic inverse spinel structure with oxygen forming a fcc closed packing

and M^{+2} and Fe^{+3} occupy either tetrahedral or octahedral sites. Magnetic configuration of MFe_2O_4 material can be engineered by adjusting the chemical identity of M^{+2} to provide a wide range of magnetic properties. [56, 63] Synthesis of ferrite nanoparticles with uniform size is the key for many applications because the magnetic properties depend strongly on their dimensions.

Recently, great efforts have been made to achieve a fine-tuning of the size of ferrite nanoparticles by using different synthesis techniques and varying experimental parameters such as heating rate and amount of surfactants. Kim and colleagues prepared cobalt ferrite nanoparticles ranging from 2 to 14 nm by controlling co-precipitation temperature of Co^{+2} and Fe^{+2} ions in alkaline solution, however, the size distribution was wide. [57] Chinnasamy's group applied a modified oxidation process to synthesize cobalt ferrite particles with diameters ranging from a few micrometers to about 15 nm. [58] Rajendrain et al. demonstrated the technique of synthesizing cobalt ferrites with sizes of 6 to 20 nm in aqueous solution at room temperature by the oxidative co-precipitation of Fe^{2+} and Co^{2+}. [59] Morais et al. shown the size-controlled synthesis of the nanoparticles of 10 to15 nm in aqueous solution at 95^{o}C by controlling stirring speed. [60] Moumen and co-workers used oil-in-water micelle to achieve the size control of Co-ferrite in the range of 2 to 5 nm. [61] Liu et al. also reported the size-controlling synthesis of Co-ferrite nanoparticles according to Moumen's micelle method but they improved the size range to 2 to 35 nm. [62] Most recently, Sun et al. synthesized ferrite nanoparticles with sizes variable from 3 to 20 nm in diameter by combining nonhydrolytic reaction with seed-mediated growth method. [63, 64]

Ferrite nanoparticles have been synthesized by a wide variety of methods as mentioned above. Although these methods are applicable to produce nano-sized ferrite particles, the quality of the nanoparticles is often poor. In many cases, a large size distribution is reported and size control is arbitrary. It is desirable to have nanoparticles of specific size and property for particular application. For example, magnetic nanoparticles must be superparamagnetic at room temperatures in order to avoid agglomeration to use as ferrofluids and in biomedical application such as MRI contrast agents. [65] However, the superparamagnetic state must be avoided in high-density information storage since the superparamagnetic relaxation of the data bits will cause the magnetic moment of each bit to fluctuate and as consequence all the stored information will be lost. Compared with other methods used for preparing ferrites nanoparticles, the chemical solution method [63, 64] has its unique advantages in producing small particles size (down to 3 nm) with very narrow size distribution, as well as good crystallinity and stability.

2.5 Applications of Magnetic Nanoparticles

High-Density Magnetic Recording - The area density of magnetic recording surpassed 10 Gbit in^{-2} in the past decade and is trying to reach the level of 1 Tbit in^{-2} in the near future. [47, 66, 67] In order to reach this ultra-high density recording, self-assembled nanoparticle media in which data are stored in an array of single-domain magnetic particles must be used to overcome the limitation of thin film media in which each bit of information is stored over hundreds of grains. Such a high-density recording media requires a very uniform size distribution and high magnetic anisotropy from

magnetic nanoparticles. [48] Synthesis and assembly of magnetic nanoparticles have great potential of being the solution of future high-density recording media. [46]

FePt $L1_0$ nanoparticles are the most promising candidate for the future magnetic recording media because of its high magnetocrystalline anisotropy, which is much higher than those of the currently used CoCr-based alloys. [68] This large crystalline anisotropy allows the thermally stable grain diameter down to 2.8 nm. [69] However, the heat treatment needed to complete the phase transition from fcc of as-synthesized particles to fct leads to agglomeration and sintering of nanoparticles, which results in poor control of orientaion of nanoparticles and limits their technological applications. [46, 71] As mentioned previously, the new technique [70] that produces monodisperse fct FePt nanoparticles with high coercivity enables the application of these hard magnetic nanoparticles in high-density recording. Other possible materials for future high-density magnetic recording include $CoFe_2O_4$ [50-52] and CoPt [72].

Nanocomposite Magnets - A nanocomposite magnet recently developed is composed of magnetically soft and hard ultra-fine grains, the magnetizations of which are coupled by the inter-grain exchange interaction. [73] Because of the presence of the soft-phase grains and the coupling of the magnetizations, nanocomposite magnets are expected to have superior hard magnetic properties, such as high remanence, coercivity and energy product. The nanocompoiste magnet was predicted to have maximum energy product $(BH)_{max}$ exceeding 100 MGOe [74] because of the exchanging coupling between soft and hard grains [9]. The hard magnetic phase provides the high anisotropy and coercivity, and the soft magnetic phase enhances the magnetic moments. The moments in

the soft grains near the interfaces are pinned to the hard grains by the exchange coupling and the centers of the soft grains can rotate in a reverse field, which results in enhanced remanent magnetization and reversible demagnetization curves because the moments of the soft grains will rotate back to align with the neighboring hard grains when the applied magnetic field is removed.

A small grain size (less than 20 nm) and a uniform mixture of the hard and soft grains are required for effective exchange coupling between the hard and the soft phases. There are two methods to accomplish the nanocomposite of hard and soft phases. In 2002, Zeng and co-workers demonstrated that exchange-coupled nanocomposite magnet of FePt-Fe_3Pt can be made by self-assembly technique using monodisperse nanoparticles of FePt and Fe_3O_4. [15] In the exchange-coupled isotropic FePt-Fe_3Pt nanocomposite, the energy product of 20.1 MGOe was achieved, which is 50% higher than the theoretical value from a single hard phase, non-exchange-coupled isotropic FePt. Another method except for self-assembly of nanoparticles is core/shell nanoparticles. Recently, the same group has prepared an exchange-coupled bimagnetic core/shell nanoparticles system with ferromagnetic FePt core and ferrimagnetic MFe_2O_4 (M=Fe, Co) shell. [54] The advantage of this core/shell system is that the magnetic properties such as magnetization and coercivity can be controlled by tuning the dimensions and therefore the material parameters of the core and shell. This system shows the great hope of achieving the predicted high energy products in exchange-coupled nanocomposite magnets. An anisotropic nanocomposite magnet with both the hard and soft phases aligned is expected to show much higher energy product than the isotropic one. [15] However, controlling

morphology including grain size and grain alignment in nanocomposite magnet remains a great challenge. [42]

Biological Applications - As the technology of magnetic nanoparticles is being developed, more and more biological applications of magnetic nanoparticles have become possible. Firstly, magnetic nanoparticles are controllable in size ranging from a few nanometers up to tens of nanometers, which matches the sizes of a cell (10-100 μm), a virus (20-450 nm), a protein (5 -50 nm) or a gene (2 nm wide and 10-100 nm long). These magnetic nanoparticles can be coated with biomoleclues and will have interaction or binding with biological entitygets when they get close to the cell or gene. New technology in molecular chemistry is trying to create true molecular magnets, in which the resulting magnets have precisely defined atomic weight and magnetic properties so that they are more compatible to biological entitygets. For example, ferritin is a natural participant in the metabolic processes of most animals, which consists of a segmented protein shell and an inner space filled with a hydrated iron oxide similar to ferrihydrite. It has been recently found that the ferrihydrite core could be replaced by magnetite and the protein shell could be reconstituted by controlling the oxidative conditions. [76] Secondly, magnetic nanoparticles can be manipulated by an external magnetic field gradient so that hey can be used to deliver a package like an anticancer drug to a targeted region in the tissue such as a tumor. Thirdly, magnetic nanoparticles can also be made to resonantly respond to a time-varying magnetic field with an associated transferred energy from the field to the nanoparticles. Therefore, these magnetic nanoparticles can be heated up, which leads to their use as hyperthermia agents, which delivers toxic amounts of

thermal energy to targeted bodies such as tumors. [16, 39-42] Other biological applications of magnetic nanoparticles include magnetic sensors and transducers and cell labeling from magnetic cell-separation techniques.

Ferrofluids - In the ferrofluid applications, magnetic nanoparticles are coated with a surfactant so that they can be prevented from agglomeration by overcoming the van der Waals forces that exists between the particles [44] and dispersed in solutions. The magnetic fluid has zero net magnetization as a result when it is not in presence of external magnetic field. When a strong magnet or magnetic field is brought close to the magnetic fluid, several spikes will appear because the fluid arranges itself along the magnetic field lines created by the magnet or the field. When the field is removed, the particles disperse again with random orientations and establish zero net magnetization. [44, 77] This property of responding to the applied magnetic field enables ferrofluids to be used in contact and hydrodynamic seals. They have low friction moments and a high degree of sealing and can be used to seal vacuum systems and high-pressure chambers, and to separate different media. Another common application of ferrofluids is the cooling of loudspeakers. The ohmic heat produced in the voice coil can be transmitted to the outer structure by the fluid that increases the cooling approximately by a factor of three.

CHAPTER 3

CHEMICAL ORDERING AND MAGNETIC ORDERING IN NANOPARTICLES

3.1 Chemical Ordering

3.1.1 Introduction

In most solid-state substances, especially for alloys, there are more than one kind of atoms in the lattice structure. In the case of binary compounds, atoms A and B are arranged on the atomic sites of the crystal lattice. When these different kinds of atoms occupy the sites randomly, we call this atomic arrangement chemically disordered. After some treatments, the A atoms may occupy in an orderly and periodic way on a certain set of atomic sites and the B atoms do similarly on another set of atomic sites. When this phenomenon occurs, we call this atomic arrangement chemically ordered and a superlattice structure is processed. There are great differences in physical and chemical properties between the disordered and ordered atomic arrangements for most of the substances. Therefore, the transition between disordered and ordered phase and the level of ordering are essentially important for the applications of the materials.

3.1.2 Long-Range Ordering

When this ordering phenomenon occurs in a large range of distance in the crystal structure, we call it long-range ordering. Let us consider a binary composition with atoms *A* and *B*. In the ordered atomic arrangement, these two kinds of atoms occupy α-sites and

β-sites, respectively. The atomic fractions of this composition are x_A and x_B, where x_A + x_B = 1. Define y_α and y_β as the fractions of α-sites and β-sites, where y_α + y_β = 1. Introduce four parameters:

r_α : fraction of α-sites occupied by the right atoms,

w_α : fraction of α-sites occupied by the wrong atoms,

r_β : fraction of β-sites occupied by the right atoms.

w_β : fraction of β-sites occupied by the wrong atoms.

where $r_\alpha + w_\alpha = 1$ and $r_\beta + w_\beta = 1$.

Because of the truth that fraction of the sites occupied by A atoms must be equal to the fraction of A atoms, and the it is the same as B atoms, we have the following relations:

$$\begin{aligned} y_\alpha r_a + y_\beta w_\beta &= x_A, \\ y_\beta r_\beta + y_\alpha w_\alpha &= x_B \end{aligned} \tag{3.1}$$

Define the long-range ordering parameter as S, which is linear to $(r_\alpha + r_\beta)$: [93, 94]

$$S = a + b\left(r_\alpha + r_\beta\right) \tag{3.2}$$

Since S = 0 for a completely disordered arrangement and S = 1 for a fully ordered arrangement, for the first condition,

$$S = a + b\left(x_A + x_B\right) = a + b = 0 \tag{3.3}$$

For the second condition,

$$S = a + 2b = 1 \tag{3.4}$$

Using equation (3.3) and (3.4), the long-range ordering parameter can be expressed in this form:

$$S = r_\alpha + r_\beta - 1 = r_\alpha - w_\beta = r_\beta - w_\alpha \tag{3.5}$$

Applying equation (3.1), then the expression of S becomes:

$$S = \frac{r_\alpha - x_A}{y_\beta} = \frac{r_\beta - x_B}{y_\alpha} \tag{3.6}$$

The long-range ordering parameter S reaches unity as its maximum value for a completely ordered atomic arrangement and any value less than unity for a partially ordered atomic arrangement. Because of the definition of S, the structure factor for the X-ray reflections of the superlattice structure is proportional to S and thus S can be calculated from experiments, where the structure factor is related to the sum of all the atomic positions in the unit cell structure. Taking both α-sites and β-sites into account, the structure factor can be defined as:

$$F = \sum_\alpha \left(r_\alpha f_A + w_\alpha f_B\right) e^{2\pi i(hx_n + ky_n + lz_n)} + \sum_\beta \left(r_\beta f_B + w_\beta f_A\right) e^{2\pi i(hx_n + ky_n + lz_n)}, \tag{3.7}$$

where f is the average scattering factor for each kind of site.

Now let us take a look at some examples of the long-range ordering in three alloy materials. Figure 3.1 shows the atomic structures of β-CuZn, Cu_3Au and CuAu I types materials when ordering occurs. In X-ray diffraction analysis, reflections that do not depend on the degree of ordering are called fundamental reflections and those that do are called superlattice reflections. The latter is the evidence of ordering.

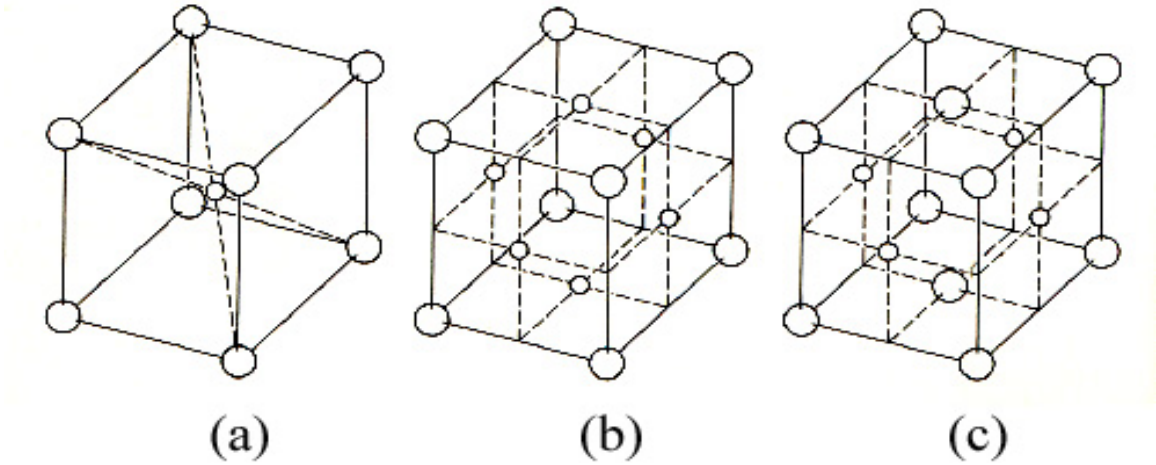

Figure 3.1 Ordered structures of (a) β-CuZn, (b) Cu_3Au and (c) CuAu

In the case of partial ordering, equation (3.1), (3.5) and (3.7) are used to get the representations of the structure factors for different types of materials.

(1) β-CuZn type:

β = (000); α = (½, ½, ½); y_α = ½; y_β = ½;

$$F = \left(r_\alpha f_A + w_\alpha f_B\right) e^{\pi i(h+k+l)} + \left(r_\beta f_B + w_\beta f_A\right),$$

If $h + k + l =$ even,

fundamental: $F = \left(r_\beta f_B + w_\beta f_A\right) + \left(r_\alpha f_A + w_\alpha f_B\right) = 2\left(x_B f_B + x_A f_A\right)$,

If $h + k + l =$ odd,

superlattice: $F = \left(r_\beta f_B + w_\beta f_A\right) - \left(r_\alpha f_A + w_\alpha f_B\right) = S\left(f_B - f_A\right)$.

(2) Cu_3Au type:

β = (000); α = (½, ½, 0), (0, ½, ½), (½, 0, ½); y_α = ¾; y_β = ¼;

$$F = \left(r_\alpha f_A + w_\alpha f_B\right)\left[e^{\pi i(h+k)} + e^{\pi i(k+l)} + e^{\pi i(l+h)}\right] + \left(r_\beta f_B + w_\beta f_A\right),$$

If *hkl* are unmixed,

fundamental: $F = \left(r_\beta f_B + w_\beta f_A\right) + 3\left(r_\alpha f_A + w_\alpha f_B\right) = 4\left(x_B f_B + x_A f_A\right)$,

If *hkl* are mixed,

superlattice: $F = \left(r_\beta f_B + w_\beta f_A\right) - \left(r_\alpha f_A + w_\alpha f_B\right) = S\left(f_B - f_A\right)$.

(3) CuAu I type:

β = (000), ((½, ½, 0); α = (½, 0, ½), (0, ½, ½); y_α = ½; y_β = ½;

$$F = \left(r_\alpha f_A + w_\alpha f_B\right)\left[e^{\pi i(h+l)} + e^{\pi i(k+l)}\right] + \left(r_\beta f_B + w_\beta f_A\right)\left[1 + e^{\pi i(h+k)}\right],$$

If *hkl* are unmixed,

fundamental: $$F = 2\left[\left(r_\beta f_B + w_\beta f_A\right) + \left(r_\alpha f_A + w_\alpha f_B\right)\right] = 4\left(x_B f_B + x_A f_A\right),$$

(3.8)

If $h + k = \text{even},\ k + l = \text{odd}$,

superlattice: $$F = 2\left[\left(r_\beta f_B + w_\beta f_A\right) - \left(r_\alpha f_A + w_\alpha f_B\right)\right] = 2S\left(f_B - f_A\right).$$

(3.9)

Having the representations of the structure factors and knowing equation (3.10), we can obtain the long-range ordering parameter S by calculating FF^*, where F^* is the complex conjugate of F.

$$I = L \times A \times D \times FF^* \tag{3.10}$$

where,

I : integrated intensity of XRD peaks,

L : Lorentz polarization factor,

A : absorption factor,

D : temperature factor.

3.1.3 Long-Range Ordering Parameter of FePt by X-ray Diffraction

The long-range ordering parameter of FePt nanoparticles can be determined by using the X-ray diffraction (XRD) method. FePt alloy belongs to the CuAu I type atomic structure. There are two different phases of FePt with different atomic structures. Figure 3.2 shows the atomic structures of face-centered cubic (fcc) and face-centered tetragonal (fct) phase FePt. For fcc phase FePt, Fe and Pt atoms occupy randomly in the atomic sites in the crystal lattice. On the other hand, they are arranged in an orderly and periodic way for fct phase FePt. For this ordered atomic structure, Pt atoms can only occupy the center layer of the lattice and Fe atoms can only occupy the other layers except the center one. The transition from fcc phase to fct phase is extremely important because there are essential and huge difference in magnetic property between these two different atomic arrangements.

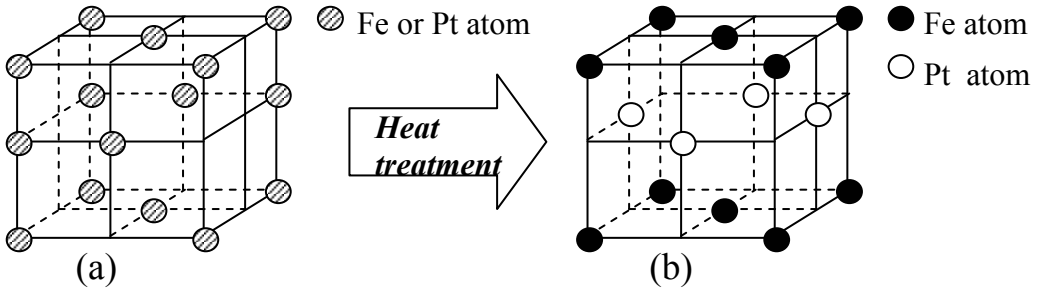

Figure 3.2 Atomic structures of (a) fcc and (b) fct phase FePt

In order to do dispersion correction to allow assuming that the sample surface is sufficiently smooth, we take the average scattering factor f as a complex number. Thus,

average scattering factor $= f + \Delta$, where f is th real part and Δ is the imaginary part. According to equation (3.8) and (3.9), [95]

$$\left(FF^*\right)_{fund} = 16\left[\left(x_{Fe}f_{Fe}e^{-M_{Fe}} + x_{Pt}f_{Pt}e^{-M_{Pt}}\right) + \left(x_{Fe}\Delta_{Fe}e^{-M_{Fe}} + x_{Pt}\Delta_{Pt}e^{-M_{Pt}}\right)\right], \quad (3.11)$$

$$\left(FF^*\right)_{super} = 4S^2\left[\left(f_{Pt}e^{-M_{Pt}} - f_{Fe}e^{-M_{Fe}}\right)^2 + \left(\Delta_{Pt}e^{-M_{Pt}} - \Delta_{Fe}e^{-M_{Fe}}\right)^2\right]. \quad (3.12)$$

Using equation (3.10), (3.11) and (3.12),

$$S^2 = \frac{\left(FF^*\right)_{super}}{\left(FF^*\right)_{fund}} \cdot \frac{4\left[\left(x_{Fe}f_{Fe}e^{-M_{Fe}} + x_{Pt}f_{Pt}e^{-M_{Pt}}\right) + \left(x_{Fe}\Delta_{Fe}e^{-M_{Fe}} + x_{Pt}\Delta_{Pt}e^{-M_{Pt}}\right)\right]}{\left[\left(f_{Pt}e^{-M_{Pt}} - f_{Fe}e^{-M_{Fe}}\right)^2 + \left(\Delta_{Pt}e^{-M_{Pt}} - \Delta_{Fe}e^{-M_{Fe}}\right)^2\right]}$$

$$= \frac{I_{super}}{I_{fund}} \cdot \frac{\left(L \times A \times D\right)_{fund}}{\left(L \times A \times D\right)_{super}} \cdot \frac{4\left[\left(x_{Fe}f_{Fe}e^{-M_{Fe}} + x_{Pt}f_{Pt}e^{-M_{Pt}}\right) + \left(x_{Fe}\Delta_{Fe}e^{-M_{Fe}} + x_{Pt}\Delta_{Pt}e^{-M_{Pt}}\right)\right]}{\left[\left(f_{Pt}e^{-M_{Pt}} - f_{Fe}e^{-M_{Fe}}\right)^2 + \left(\Delta_{Pt}e^{-M_{Pt}} - \Delta_{Fe}e^{-M_{Fe}}\right)^2\right]}$$

Allowing the approximation, [96]

$$S \cong 0.85 \cdot \left(\frac{I_{super}}{I_{fund}}\right)^{\frac{1}{2}} \quad (3.13)$$

Equation (3.13) is an approximate method to obtain S based on the previous studies of long-range ordering parameter. [93-96] This method uses the ratio of integrated intensities of the superlattice peak to the fundamental peak from XRD patterns. The low-order fundamental reflections are much stronger than the superlattices reflections, and their measured values tend to be too small due to extinction; hence, we prefer to use the weaker high-order fundamentals when calculating *S*. [93]

3.1.4 Long-Range Ordering Parameter by Transmission Electron Microscope

Transmission electron microscope (TEM) is another method to determine the long-range ordering parameter *S* other than XRD. The scattering amplitude of atoms for electrons is much larger than that for X-rays. Therefore, electron diffraction has greater ability to pick up signals of fundamental and supperlattice reflections from small volume of ordered nanoparticles than XRD. [98-100] The advantage of this method is that it can characterize the ordering information of a particular single nanoparticle.

In this method, the electron diffraction pattern of the sample is obtained on the image plates from TEM. Quantitative analysis of diffraction beam intensities is carried out according to the exposure time and similarly to XRD method, the ratio of the intensities of the superlattice to the fundamental is used to determine *S*. However, the strong interaction between electrons and nanoparticles creates multiple scattering instead of single scattering that is interpreted by XRD method, which makes the normal analysis of using ratios of intensities incorrect. Previous studies show that the multislice approach must be used to simulate the transmission behavior of electrons through crystals and calculate the intensities of propagating electrons. [97-100] In this approach, experimental parameters such as specimen thickness, incident-beam direction, specimen composition, lattice parameters are to be considered. Computer softwares that perform the multislice similation, such as “Mac Tempas”, calculate the final intensities of superlattice and fundamental and the long-range ordering parameter. [99] In these studies of *S* by electron diffraction, the particles are usually c-axis oriented perpendicular to the specimen plate due to the method of producing the particles. Hence, [110] and [220] reflections are used

for superlattice and fundamental, respectively. This TEM method gets involved with computational simulations and clarifies the corresponding relationship between intensity ratios and long-range ordering parameters.

3.1.5 Size-Dependent Chemical Ordering of FePt Nanoparticles

It has been found that the chemical ordering of FePt nanoparticles is strongly dependent on particle size. Under the assumption that the system is isotropic and of the same composition, and the particle shape is spherically symmetrical, the long-range ordering parameter *S* should obey the Euler equation in spherical coordinators. [109]

$$2\kappa_s \frac{d^2S}{dr^2} + \frac{4\kappa_s}{r}\frac{dS}{dr} = \frac{\partial \Delta f}{\partial S}$$

with the boundary conditions,

$$\frac{dS}{dr} = 0 \text{ at } r = 0$$

and

$$S = 0 \text{ at } r = \frac{d}{2},$$

where κ_s is the gradient energy coefficient of ordering parameter *S* and *d* is the diameter of FePt nanoparticles. This second-order differential equation is solved numerically for various values of particle diameter *d*. The calculation shows that the proportional relation exists between long-range ordering parameter *S* and particle diameter *d*. Moreover, this calculation also predicts that there will be a critical particle size below which long-range ordering can not complete. Monte Carlo simulations can be used to demonstrate the size-dependent long-range ordering parameter of FePt nanoparticles theoretically. [112, 113]

Takahashi and co-workers experimentally proved the size-dependence of ordering in FePt nanoparticles by TEM characterization of FePt nanoparticles deposited on Al_2O_3 films. [109, 110] Miyazaki and colleagues also concluded similar result for the FePt nanoparticles grown on MgO films. [111] According these previous studies, the critical size is within a range between 2.5 to 4 nm. [109-113] All these previous works of size-dependent long-range ordering can only provide the local ordering information in a very limited area of a sample with similar particle sizes because the particle size distribution is wide. Universal long-range ordering study must be conducted in a sample with narrow particle distribution, which represents the ordering information of the particular particle size. Method that produces chemically ordered FePt nanoparticles with narrow size distribution is desired for more accurate size-dependent long-range ordering study.

3.2 Magnetic Ordering

3.2.1 Introduction

If there is no magnetic interaction between individual magnetic moments, in the absence of a magnetic field, the vector moment of each magnetic ion in solid materials will average to zero. Nevertheless, as we discussed in the previous chapter, there exists magnetic orderings in some solid materials. In such types of materials, individual magnetic ions have non-vanishing average vector moments even in the absence of external magnetic field below a critical temperature, and this phenomenon is called magnetic ordering of solid materials.

Individual localized moments in a magnetically ordered solid material may or may not add up to a net magnetization as a whole. If they do, the microscopic magnetic

ordering is revealed by the existence of a macroscopic bulk magnetization that is known as spontaneous magnetization and this type of ordered materials is called ferromagnetic material. As described in figure 1.2, the magnetic moments in a ferromagnetic material have the same orientation and magnitude in the absence of external fields so that their summation causes a non-zero spontaneous magnetization. The more common case in solid materials is that the sum of the individual localized moments is zero in a magnetically ordered material, which results in zero spontaneous magnetization from the microscopic ordering. Such type of ordered materials is called antiferromagentic material and its magnetic moments have the same magnitude but in two groups pointing to opposite orientations, because of which the magnetic moments cancel out by themselves, resulting in zero total magnetization. In ferromagnetic materials, all local moments have a positive component along the direction of the spontaneous magnetization to generate a non-zero spontaneous magnetization. Solid materials that are able to generate non-zero spontaneous magnetization but fail to satisfy this criterion is called ferrimagnetic material. In this kind of materials, the exchange coupling between nearest neighboring moments intend to align in an antiparallel manner, however, these neighboring moments are not identical in magnitude and will not cancel out, which leaves a net non-zero spontaneous magnetization.

3.2.2 Thermodynamic Properties at the Onset of Magnetic Ordering

As discussed in the previous chapter, the critical temperature above which magnetic ordering vanishes is called Curie temperature (T_c) in ferromagnetic or ferrimagnetic materials and Néel temperature (T_N) in antiferromagnetic materials. Below

these critical temperatures, magnetic ordering, no matter parallel or antiparallel arrangement, exists as the nature of the materials because of the exchange interaction between neighboring magnetic moments. As the temperature is approaching to the critical temperature from below, the thermal energy is becoming sufficient to overcome the exchange interaction between magnetic moments. Once the temperature reaches the critical temperature, the magnetic ordering disappears completely. In the case of ferromagnetic or ferrimagnetic materials, spontaneous magnetization decreases to zero continuously. The observed magnetization just below Curie temperature T_c can be described in a power law,

$$M(T) \sim (T_c - T)^{\beta}$$

where β is typically in the range from 0.33 to 0.37. [101-102] The onset of magnetic ordering can be also demonstrated by the zero-field susceptibility as the temperature decreases to Curie temperature T_c from above. In most cases, the susceptibility varies inversely with T at all temperatures. However, in ferromagnetic materials, the susceptibility is observed to diverge as T decreases to T_c and follows,

$$\chi(T) \sim (T - T_c)^{-\gamma},$$

where γ is typically between 1.3 and 1.4. [101, 103]

3.2.3 Curie Temperatures of Nanoparticles

In the case of nanoparticles, Curie temperature has been found to decrease as the particle size decreases. This size-dependent behavior of Curie temperature of nanoparticles is based on the condition of similar microstructure and composition of

materials because they are also effective factors of Curie temperature other than particle size. Satisfying this condition, the reason for this behavior of nanoparticles can be described by the finite size scaling theory, [104]

$$\frac{T_c(\infty)-T_c(d)}{T_c(\infty)}=\left(\frac{d}{d_0}\right)^{-\frac{1}{\upsilon}} \tag{3.14}$$

where $T_c(d)$ is the Curie temperature as a function of particle size d, $T_c(\infty)$ is the bulk Curie temperature, d_0 is a constant and υ is the critical exponent of the correlation length. The finite size scaling theory predicts the shift in the transition temperature from that of the bulk depends on the size of the system. In other words, the decreasing particle size results the decline in the Curie temperature, which indicates that magnetic ordering of smaller nanoparticles disappears at a lower temperature than bigger nanoparticles. [104-106] Moreover, this size-dependent behavior of Curie temperature also implies that the coupling interactions between neighboring magnetic moments that cause the magnetic ordering in smaller particles are weaker than that in bigger particles so that thermal energy can more easily overcome the interactions. On the other hand, this behavior is observed to be consistent with the long-range chemical ordering of nanoparticles. In most cases, more ordered atomic arrangement causes more ferromagnetic or ferrimagnetic phases and results in stronger coupling interactions between magnetic moments, which is the origin of magnetic ordering. Therefore, more developed long-range chemical ordering of nanoparticles results in more stable magnetic ordering, which is characterized by higher Curie temperatures. [107, 108]

CHAPTER 4

EXPERIMENTAL PROCEDURES AND EQUIPMENTS

4.1 Synthesis of FePt Nanoparticles

FePt nanoparticles were synthesized by chemical reduction of platinum acetylacetonate ($Pt(acac)_2$) and iron pentacarbonyl ($Fe(CO)_5$) or iron acetylacetonate ($Fe(acac)_3$) as iron precursor, with or without 1,2-hexadecanediol at high temperature in solution phase in standard airless argon atmosphere. FePt particles with diameters from 2 to 15 nm can be synthesized by varying precursors, amount of surfactants and heating rate of the system. [14, 17-19]

As shown in figure 4.1, the typical synthesis route of 4 nm FePt nanoparticles followed Sun's method. [14] Platinum acetylacetonate (197 mg, 0.5 mmol), 1,2-hexadecancediol (390 mg, 1.5 mmol), and dioctylether (20 ml) were mixed and heated to 100 ^{o}C in argon atmosphere. Then oleic acid (0.16 ml, 0.5 mmol), oleylamine (0.17 ml, 0.5 mmol) and $Fe(CO)_5$ (0.13 ml, 1 mmol) were injected, and the mixture was heated to the reflux temperature (295 ^{o}C). The refluxing was processed for 30 minutes. The heat source was then removed and the reaction mixture was allowed to cool down to room temperature. The purification of nanoparticles was carried out by centrifugation in hexane and ethanol at 6000 rpm for 10 minutes. This purification process was repeated 3 times at least and the purified FePt nanoparticles were then re-dispersed in hexane.

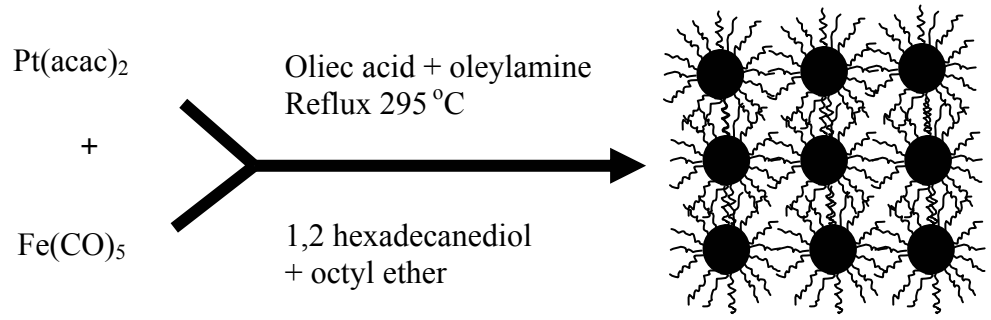

Figure 4.1 Scheme for synthesis of FePt nanoparticles

Synthetic parameters were adjusted to synthesize FePt nanoparticles with diameters other than 4 nm. Normally, only FePt nanoparticles larger than 4 nm can be synthesized by $Fe(CO)_5$ as iron precursor. By changing the iron precursor from $Fe(CO)_5$ to $Fe(acac)_3$ and keeping the rest of the synthetic conditions the same, FePt particles with average size of 2 nm could be produced. Surfactants typically play crucial role in modifying nanoparticle size. The molar ratio of surfactants:$Pt(acac)_2$ was observed to affect the particle size. When the reaction heating rate was maintained at 5ºC/min, particles with average size of 4 nm was obtained if the molar ratio was 1:1, while particles size increased to 8 nm if the ratio was increased to 4:1. Another factor that affects the particle size is the heating rate. Keeping all the other synthetic parameters constant in the 8 nm particle synthesis, if the heating rate was increased from 5 to 15ºC/min, the average size of FePt particles decreased from 8nm to 6 nm. FePt particles larger than 8 nm could only be made indirectly. 10 nm Pt cores were synthesized by addition of Pt precursor at 290°C in a mixture of octyl ether and surfactants. Then the

particles were coated with iron to make 15 nm Pt/Fe3O4 core-shell particles. This kind of particles could be converted to FePt after annealing.

4.2 Salt-Matrix Annealing Technique

As mentioned in 2.3, as-synthesized FePt nanoparticles have to be heat-treated at a temperature higher than 500^{o}C to be converted from fcc chemically disordered phase to fct chemically ordered phase. Salt-matrix annealing technique was used to process this heat treatment and prevent sintering and agglomeration of nanoparticles during heat treatment.

Firstly, sodium chloride (NaCl) was chosen to be the separating media due to its high chemical stability. The NaCl powder with particle size less than 10 μm was prepared by mechanical surfactant-assisted ball milling. A 500 ml Nalgene high-density polyethylene plastic container was inserted into a stainless steel container as shown in figure 4.2. And then the milling mixture as shown below was loaded into the plastic container.

- 50 grams of NaCl powder,
- 500 grams of 10 mm in diameter 316 stainless steel balls, ball to powder weight ratio is 10:1,
- 200 ml of heptane,
- 20 ml of surfactant (oleyl amine), 10% of heptane.

The mixture was milled for 24 hours and the dispersion of NaCl in heptane with the assistance of surfactant was obtained.

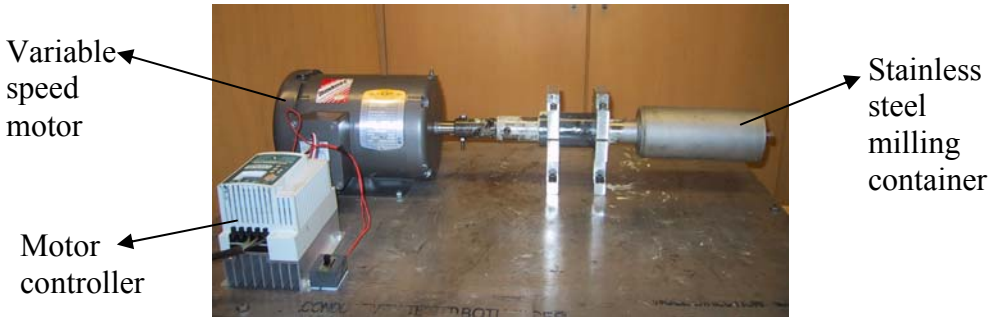

Figure 4.2 The ball milling set-up for milling of NaCl powders

Secondly, as-synthesized FePt nanoparticles dispersed in hexane was mixed with NaCl dispersion in heptane. The weight ratio of NaCl to FePt was varied, from 1:1 to 400:1. A Büchi R-200 rotary evaporator as shown in figure 4.3 was used to achieve homogeneous mixing and evaporation of solvents. After all the solvents were evaporated, dry mixture of FePt in NaCl matrix was obtained. Milling and crushing of the dry mixture was then performed by using a marble and a pestle.

Figure 4.3 Büchi R-200 rotary evaporator

Thirdly, the homogeneous mixture was annealed in forming gas (93% H_2 + 7% Ar_2) in different conditions from 600 to 750 ^oC for 2 to 8 hours to investigate the fcc-to-fct transition by using a Lindberg Blue-M tube furnace. After annealing, the mixture was then washed by de-ionized water for at least three times to remove NaCl. Centrifugation at 6000 rpm for 2 minutes was used to separate the FePt nanoparticles from the water. Acetone was used to absorb the remaining water and centrifugation was again applied to get separated FePt nanoparticles. Finally, these annealed FePt nanoparticles could be re-dispersed in cyclohexane with the assistance of surfactants.

4.3 Characterization Techniques

4.3.1 X-ray Diffraction (XRD)

Philips PW 1710 X-ray diffractometer with Cu-Kα radiation (wavelength λ=1.54056 A^o) was used for crystalline structure characterization of samples. The samples were prepared by depositing nanoparticles on glass substrate and X-ray was applied on the sample. The incident X-ray follows Bragg's law as described in figure 4.4 and the following formula: [94]

$$n\lambda = 2d\sin\theta ,$$

when a monochromatic X-ray beam with wavelength λ is projected onto a crystalline material at an angle θ, diffraction occurs only when the distance traveled by the rays reflected from successive planes differs by a complete number n of wavelengths. By varying the angle θ, the Bragg's Law conditions are satisfied by different d-spacings in materials. Plotting the angular positions and intensities of the resultant diffracted peaks of radiation produces a pattern that is characteristic of the sample. Usually 2θ is used instead

of θ. When a mixture of different phases is present, the resultant diffractogram is formed by addition of the individual patterns.

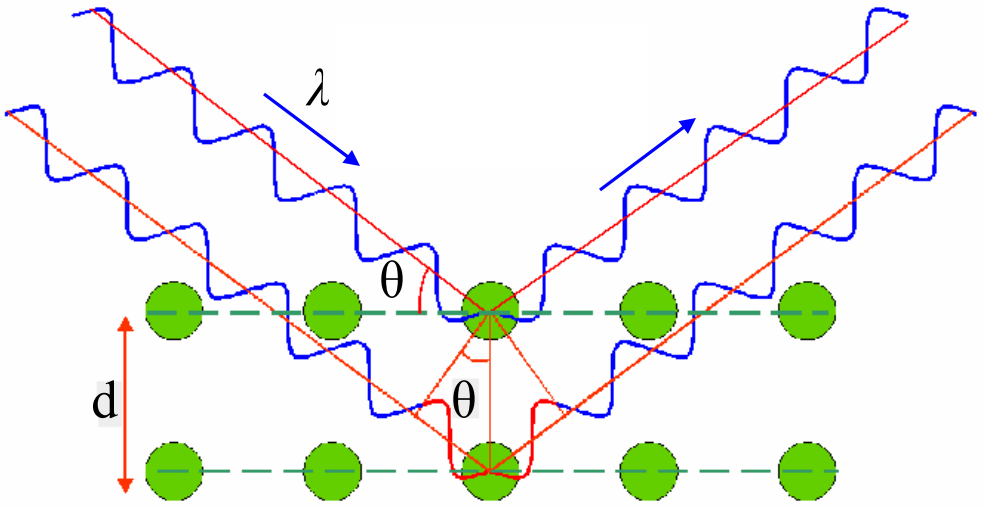

Figure 4.4 Bragg's law

4.3.2 Transmission Electron Microscope (TEM)

JEOL's 1200EX TEM was used for observing the morphologies and crystalline structure of nanoparticles. This TEM uses an acceleration voltage of 120 kV and can reach a magnification up to 500k times. Bright field images as well as the selected area electron diffraction (SAED) patterns were captured onto negative films, which were then developed and scanned as digital images.

A 300-mesh copper grid with a carbon film deposited on a formvar backing, purchased from Ted Pella, were used for preparing TEM samples. A drop of the nanoparticle dispersion solution in octane was put on the formvar side of the TEM grid and the solvents were allowed to evaporate in air. Formvar is more hydrophobic than carbon and hence the solvent (octane is also hydrophobic) can spread out easily on the

grid instead of staying agglomerated in the form of a small drop. Thus, nanoparticles coated with surfactants can assemble on the grid. However, for TEM imaging of nanoparticles, it is important to avoid excessive surfactant coating, which causes difficulties for the electron beam to transmit through the sample, therefore reduce the contrast and quality of the observation of nanoparticles.

Figure 4.5 shows a typical structure of a conventional TEM. The high acceleration voltage generates electrons that are collected by the condenser lenses. The electron beam then transmits through the specimen and the objective lens creates images of the specimen. Projective lens then projects the image onto the fluorescent screen. By tuning the objective lens and projective lens, magnification and focus can be adjusted respectively. Images are recorded on the negative films by the camera installed at the bottom portion of the TEM. In the image mode of TEM, if transmitted beam of electrons through the specimen is chosen to create images, then it is called bright field image. On the other hand, it is called dark field image if the diffracted beam is chosen. The selected area electron diffraction (SAED) pattern will be shown if the diffraction mode of TEM is set.

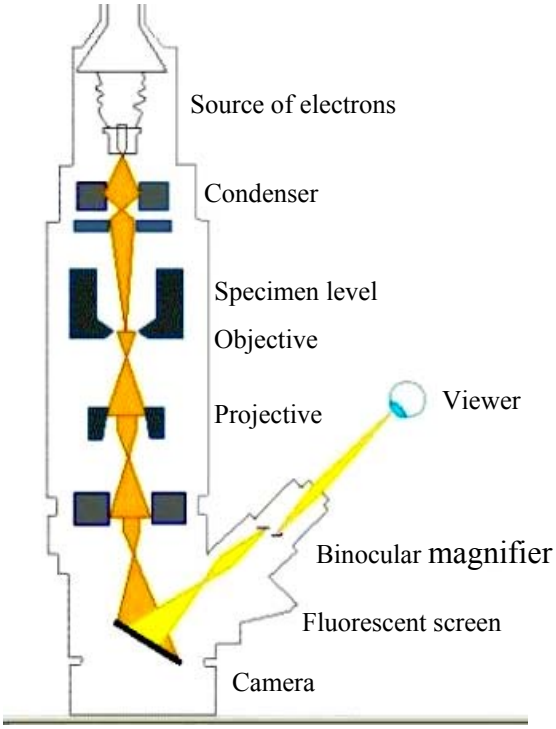

Figure 4.5 Structure of the conventional TEM

4.3.3 High-Resolution TEM (HRTEM)

High-resolution TEM imaging of selected samples were performed by Hitachi HF 2000 TEM at Georgia Institute of Technology. Sample preparation for HRTEM analysis is the same as that for TEM.

4.3.4 Compositional Characterization

Inductively coupled plasma-optical emission spectroscopy (ICP-OES) analysis on composition of selected samples was processed by Galbraith Research Labs. Powder samples were prepared and sent for ICP-OES analysis.

4.3.5 Magnetic Measurements

4.3.5.1 Sample Preparation for Magnetic Measurements

Samples for magnetic measurements were prepared by depositing a few drops of the final dispersion of nanoparticles on a 3 × 3 mm silicon substrate and evaporating the solvents at room temperature, which led to the formation of nanoparticle assemblies on the substrates. The samples were then dried in a vacuum to remove volatile organics from the assemblies. Epoxy as the binder was used to prevent nanoparticles from motion during magnetic measurements. In the case of fct FePt nanoparticles, samples were also prepared by mixing nanoparticles with epoxy or PVC as binder on Si substrates, or by freezing nanoparticle-dispersions in alcohol or water, with or without magnetic field alignment. Hardened epoxy or PVC and frozen solvents provide accurate magnetic measurements of nanoparticles by avoiding nanoparticle motions while magnetic filed is applied.

FePt nanoparticles embedded in salt-matrix right after annealing were prepared as the samples for Curie temperature measurements in order to avoid grain growth of nanoparticles when high temperature was applied during M-T measurements. The samples without protection of salt-matrix were also measured for the purpose of comparison.

4.3.5.2 Alternating Gradient Magnetometer (AGM)

In an AGM measurement, the sample is mounted on an extended rod attached to a piezoelectric element and then placed at the center of the poles that generates magnetic field. The sample is magnetized by a static DC field and an alternating gradient magnetic

field produces an alternating force that applies on the sample. This force (F) is proportional to the magnitude of the alternating magnetic field (Mag) and the magnetic moment (M) of the sample. Thus,

$$F \propto (Mag)\,\&\,(M)$$

If (Mag) is kept constant,

$$F \propto M\ .$$

This force is converted into a proportional voltage by a piezoelectric element and hence the moment of the sample can be measured. The applied field is measured by a Hall probe sensor and the sensitivity of the AGM can reach up to 10 nemu. Samples with dimension up to 5 mm x 5 mm can be measured in AGM. The maximum magnetic field that can be applied by AGM is limited to 14 kOe and it can only be operated at room temperature. Therefore, samples that have high anisotropy or require low or high temperature measurements will need magnetometers that can provide much higher saturation field to get accurate magnetic measurements and capability of operating in different temperatures.

4.3.5.3 Superconducting Quantum Interference Device (SQUID) Magnetometer

SQUID uses a superconducting magnet, through which large amount of current can flow so that large magnetic field can be generated. The magnetic measuring mechanism of SQUID belongs to inductive technique. During magnetic moment measurement, the sample moves through a system of superconducting detecting coils and the magnetic moment of the sample causes change in magnetic flux associated with the detecting coils, resulting in electric current produced in the detecting coils. The detecting

coils are connected to the SQUID sensor, which functions as a highly linear current-to-voltage converter, producing very accurate variations in the output voltage that is proportional to the moment of the sample. SQUID can generate a magnetic field as high as 70 kOe and can be operated in temperatures from 2 K to 400 K. The sensitivity of SQUID is 10 nemu up to applied field of 2.5 kOe and 0.6 μemu above that. Liquid helium is required to operate SQUID, which makes the use of it expensive. Sample dimension requirement of SQUID is almost the same as AGM, but the sample for SQUID can be longer in one of its dimensions. AGM is much easier, faster, and less expensive to operate comparing to SQUID. Hence, room-temperature measurements of all samples that can be saturated below 14 kOe should be measured by AGM.

4.3.5.4 Vibrating Sample Magnetometer (VSM)

VSM is an integrated magnetometer in Physical Property Measurement System (PPMS). It can generate a magnetic field as high as 140 kOe and provide a magnetic moment sensitivity up to 1 μemu. The magnetic measuring mechanism of VSM also belongs to inductive technique and is similar to SQUID except that the motion of sample in detecting coils for VSM is much faster than SQUID. The normal operating temperature of VSM is from 1.9 K to 400 K, however, a VSM with an oven option can be operated from room temperature to 1000 K. The measurement of VSM is faster than SQUID but with lower sensitivity. Measurements that require saturation field higher than 70 kOe and temperatures higher than 400 K are performed by VSM instead of SQUID.

CHAPTER 5

RESULTS AND DISCUSSIONS

5.1 Long-Range Ordering of FePt Nanoparticles

5.1.1 Phase and Compositional Analysis

As described in 4.2, monodisperse face-centered tetragonal (fct) FePt nanoparticles were prepared by salt-matrix annealing technique. The as-synthesized FePt nanoparticles with different diameters embedded in salt-matrix were annealed in forming gas in different conditions to investigate the relation between annealing conditions and the chemical ordering. Figure 5.1 shows the XRD patterns of FePt nanoparticles with diameters from 4 to 15 nm annealed in salt-matrix at 600 ^{o}C for 2 hours and 700 ^{o}C for 2 and 4 hours. As shown in the patterns, (001) and (110) peaks, which is characteristic for chemically ordered fct FePt phase, started to develop when the particles were annealed at 700 ^{o}C for 2 hours. These XRD peaks that appear only in ordered phase are called superlattice peaks. As the annealing time increased to 4 hours, superlattice peaks (001) and (110) were more developed, indicating that the fcc-to-fct transition was more complete. The position of peaks shifts to the high-angle direction as the transition is more complete, most obviously for the (111) peaks, which is caused by the lattice length change when atomic structure changes from fcc to fct. 4 nm FePt particles were selected to run heat treatments at 700 ^{o}C for extended time. Figure 5.2 shows the XRD patterns of

4 nm FePt particles annealed 700 ^{o}C for 6 and 8 hours. No obvious evidence can be found that longer annealing time (>4 hours) can further develop the transition.

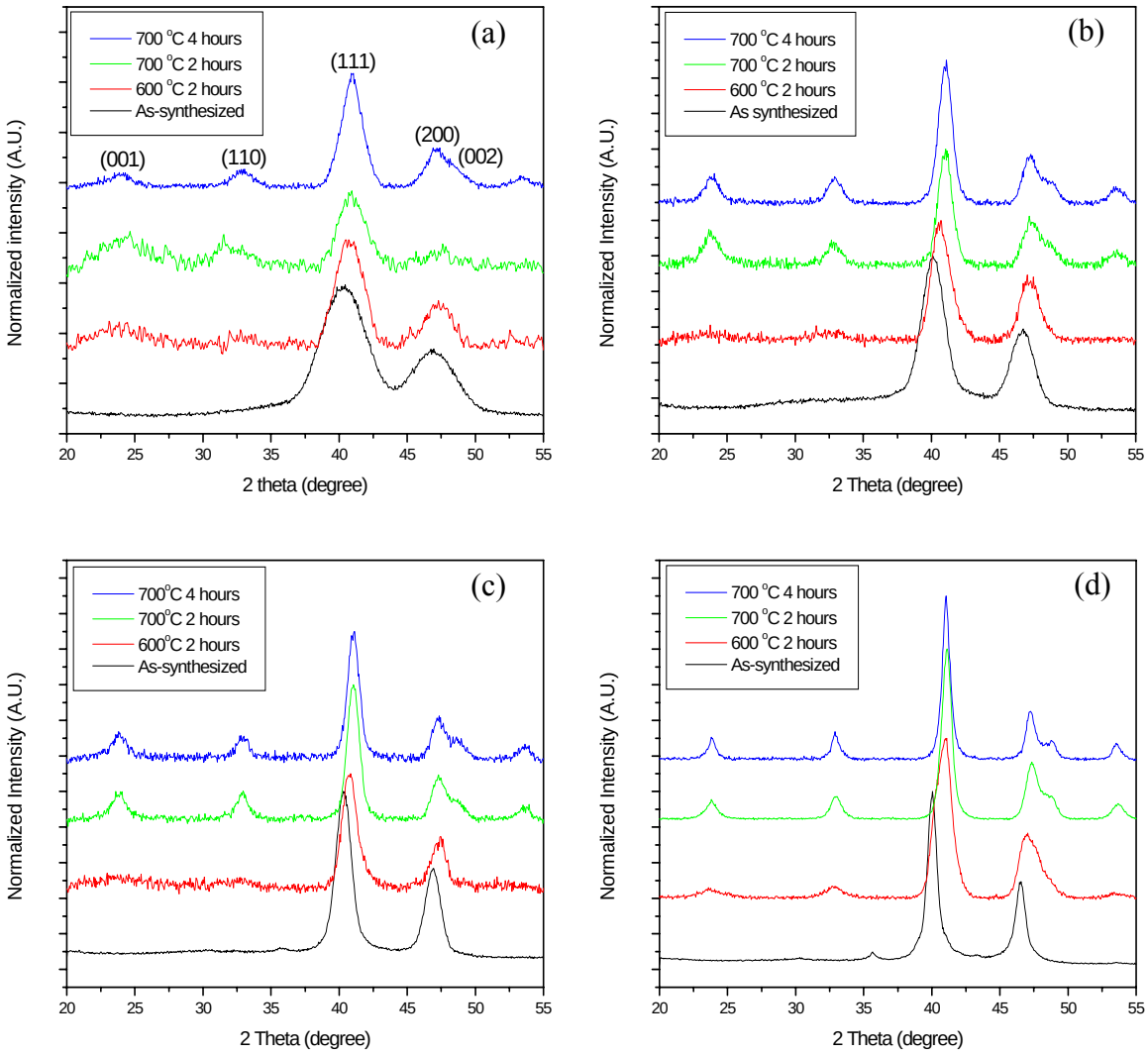

Figure 5.1 XRD patterns of as-synthesized and annealed FePt nanoparticles with diameters of (a) 4 nm, (b) 6 nm, (c) 8 nm and (d) 15 nm

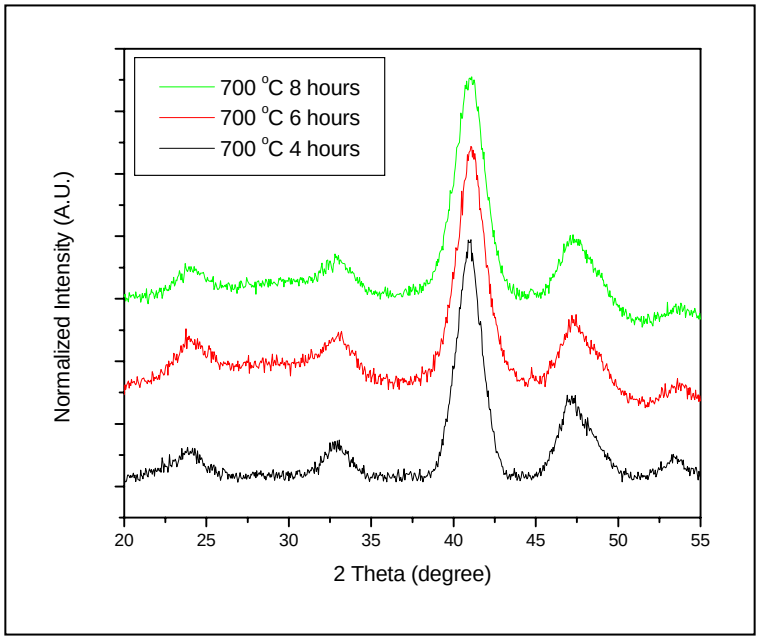

Figure 5.2 XRD pattern of 4 nm FePt nanoparticles annealed at 700 °C for 4, 6 and 8 hours

In the case of 2 nm FePt particles, the electron diffraction of TEM has to be used to perform the phase identification instead of XRD for the reason that no XRD peaks were obtained because the grain size is too small for XRD analysis. Figure 5.3 is the selected area electron diffraction images of 2 nm FePt nanoparticles annealed at 600 °C for 2 hours and 700 °C for 4 and 8 hours. Only (111) and (200) fundamental electron diffraction rings can be found and all superlattice rings are missing in all these selected area electron diffraction images, which indicates that the fcc-to-fct transition did not occur even when the 2 nm FePt nanparticles were annealed at 700 °C for 8 hours in salt-matrix. This result is consistent with the previous studies that FePt nanoparticles below a critical size limit could not be converted to fct phase. [109-111, 113]

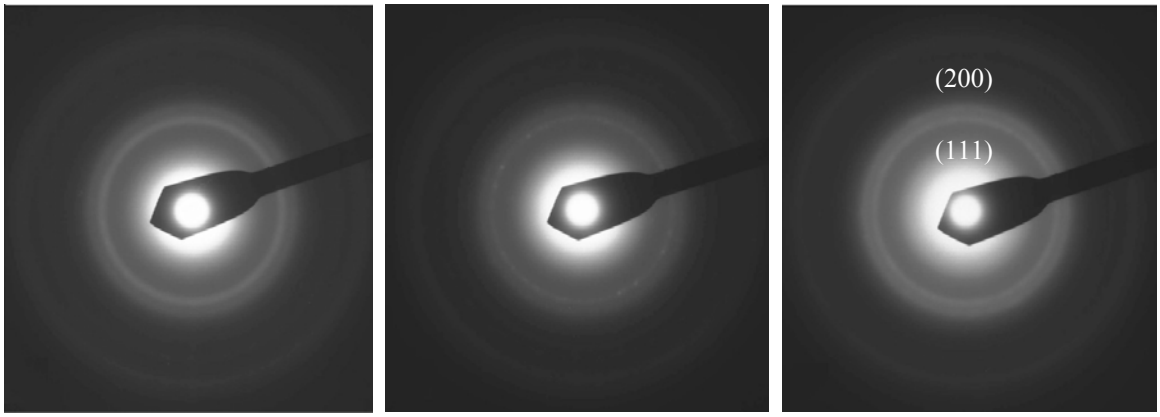

(a) (b) (c)

Figure 5.3 Selected area electron diffraction patterns of 2 nm FePt nanoparticles annealed at (a) 600 ^{o}C for 2 hours, (b) 700 ^{o}C for 4 hours and (c) 700 ^{o}C for 8 hours

In the XRD patterns, there are no peaks for the separating media NaCl, which means that the water-washing technique effectively removed the salt-matrix after annealing. ICP-OES confirmed that the NaCl level is as low as 0.099% in weight and the average composition of the nanoparticles is $Fe_{52}Pt_{48}$. Therefore, salt-matrix annealing technique can produce fct phase FePt particles without any non-magnetic impurities. From the following discussions, we will see that these fct FePt particles are monodisperse and size/shape-retained as the as-synthesized nanoparticles.

The equation below is the Scherrer equation from which grain size of XRD samples can be calculated. [93, 94]

$$L = \frac{0.94\lambda}{B(2\theta)\cos\theta}$$

where L is the crystal dimension, λ = 0.154056 nm is the wavelength of the X-ray, $B(2\theta)$ is the full width in radians subtended by the half-maximum intensity width of the peak at

angle θ. The (111) peaks were chosen to calculate the grain sizes as demonstrated by figure 5.4. The average grain sizes of FePt nanoparticles annealed at 700 ^{o}C for 4 hours are 4.7 nm, 6.8 nm, 8.2 nm and 13.3 nm for 4 nm, 6 nm, 8 nm and 15 nm particles, respectively. These grain sizes of the 4 nm, 6 nm and 8 nm particles also represent the particle sizes because all of them are of single-crystalline structure. The relatively smaller grain size of 15 nm is due to the polycrystalline structure of the 15 nm FePt nanoparticles. (See 2.5.1) Thus, salt-matrix annealing can complete the fcc-to-fct transition and prevent the grain growth during heat treatment at the same time.

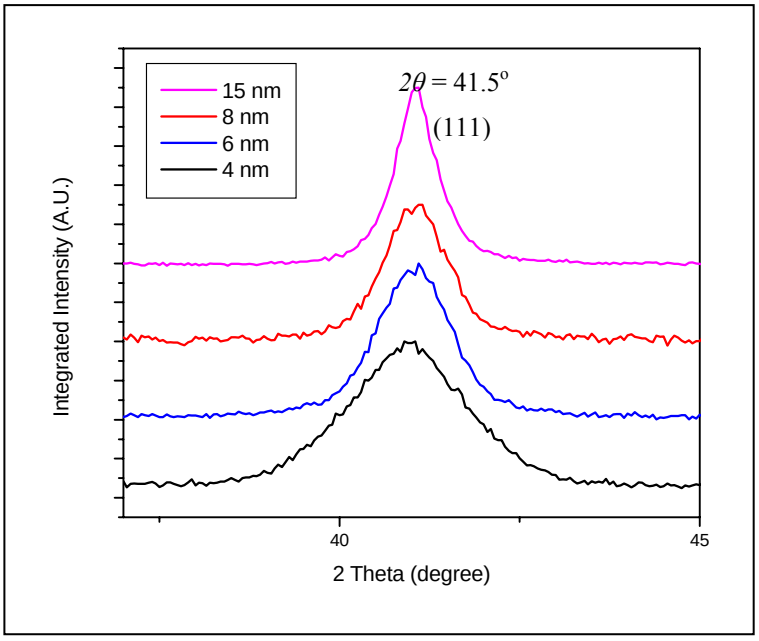

Figure 5.4 (111) XRD peaks of 4 nm, 6 nm, 8 nm and 15 nm FePt nanoparticles annealed at 700 ^{o}C for 4 hours

5.1.2 Long-Range Ordering Parameter

As we discussed in 3.1.3, the long-range ordering parameter of FePt nanoparticles can be calculated by equation 3.13. In X-ray diffraction, the low-order fundamental

reflections are much stronger than the superlattice reflections, and their measured values tend to be very small due to extinction. Hence, we prefer to use the weaker high-order fundamentals when calculating S. [93] Following the previous study of long-range ordering parameter of FePt nanoparticles, (001) and (002) were selected as the superlattice and fundamental peaks, repectively. [96] Thus, the long-range ordering parameter of our FePt nanoparticles is represented in the equation below.

$$S \cong 0.85 \cdot \left(\frac{I_{001}}{I_{002}} \right)^{\frac{1}{2}}$$

where I_{001} and I_{002} are the integrated intensities of (001) and (002) peaks, respectively. From this equation, the long-range ordering parameter of FePt nanparticles with different diameters annealed in different conditions were calculated and plotted as shown in figure 5.5. As the annealing temperature or time increases, the long-range ordering parameter *S* increases for specific particle size, which indicates that chemical ordering of FePt is more complete with increasing annealing temperature or time. *S* vanishes for 2 nm FePt nanoparticles because no (001) superlattice structure was found in the SAED patterns as shown in figure 5.3. According to figure 5.5, as the particle diameter increases from 4 to 8 nm, the long-range ordering parameter *S* increases as well, which follows the size-dependent theory of long-range ordering parameter discussed in 3.1.5. The long-range ordering parameter of 15 nm FePt nanoparticles is lower than that of the 8 nm particles, which may be due to the polycrystalline structure of the large particles. The grain boundaries in a 15 nm FePt nanoparticles may play the role of holdback in the process of chemical ordering. The *S* of 4 nm, 6 nm, 8 nm and 15 nm FePt nanoparticles annealed at

700 °C for 4 hours is 0.85, 0.92, 0.98 and 0.94, respectively, which are the maximum *S* values obtained for particular particle sizes in our experiment.

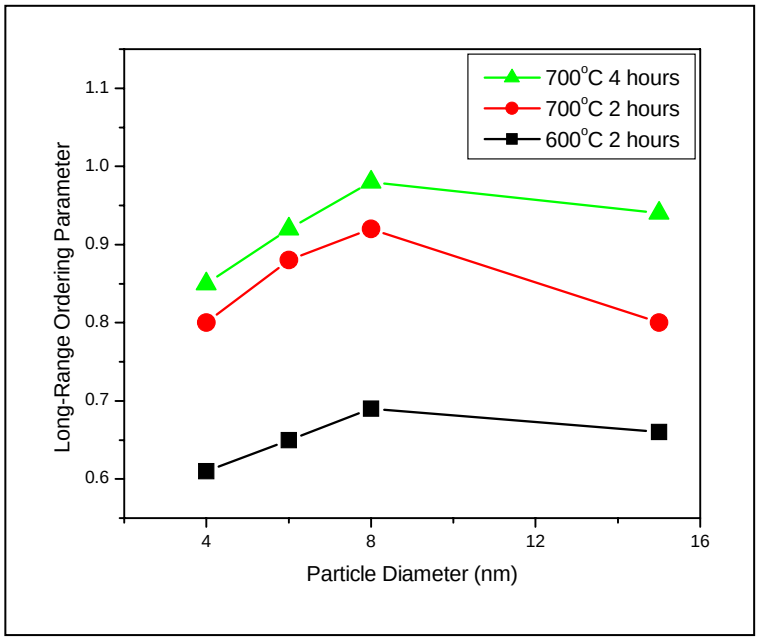

Figure 5.5 Long-range ordering parameter vs. particle diameter for different annealing conditions

Our analysis shows that the long-range ordering parameter *S* increases when the annealing temperature or time increases, or the particle size increase. When the FePt particle size is 8 nm and the annealing condition is 700 °C for 4 hours, *S* almost reaches unity, which is for the perfect chemical ordering.

5.2 Morphology of fct FePt Nanoparticles

5.2.1 TEM Analyse

TEM was used to observe the morphology of the fct FePt nanoparticles obtained from salt-matrix annealing technique. Figure 5.6 (a), (b) and (c) show the TEM images of fct FePt with diameters of 15 nm, 8 nm and 4 nm annealed in salt-matrix at 700 °C for 2

hours. From these TEM images, we can see all these fct phase FePt nanoparticles after being annealed are monodisperse and their size distribution is very narrow. As described in the HRTEM image in figure 5.6 (d), after salt-matrix annealing, 8 nm fct FePt nanoparticles remained the same cubic shape as the as-synthesized particle, which indicates that this technique can retain particle size as well as particle shape. The HRTEM images (figure 5.6 (d) and (e)) also show clearly the crystalline lattices of 4 nm and 8 nm fct FePt nanoparticles, which are of single-crystalline structure. On the other hand the HRTEM image in figure 5.7 shows that the 15 nm fct FePt nanoparticles are of polycrystalline structure, which was probably caused by the core-shell structure of the as-synthesized particles (discussed in 4.1). After salt-matrix annealing, the Fe_3O_4 shell was reduced and sintered into the Pt core of the particle, and formed polycrystalline FePt nanoparticle. There are several crystal grains in a nanoparticle, having different magnetocrystalline orientations, which is the reason why 15 nm FePt nanoparticles have relatively lower chemical ordering (discussed in 5.1.2) and anisotropy (discussed in 5.3) compared to particles with other sizes.

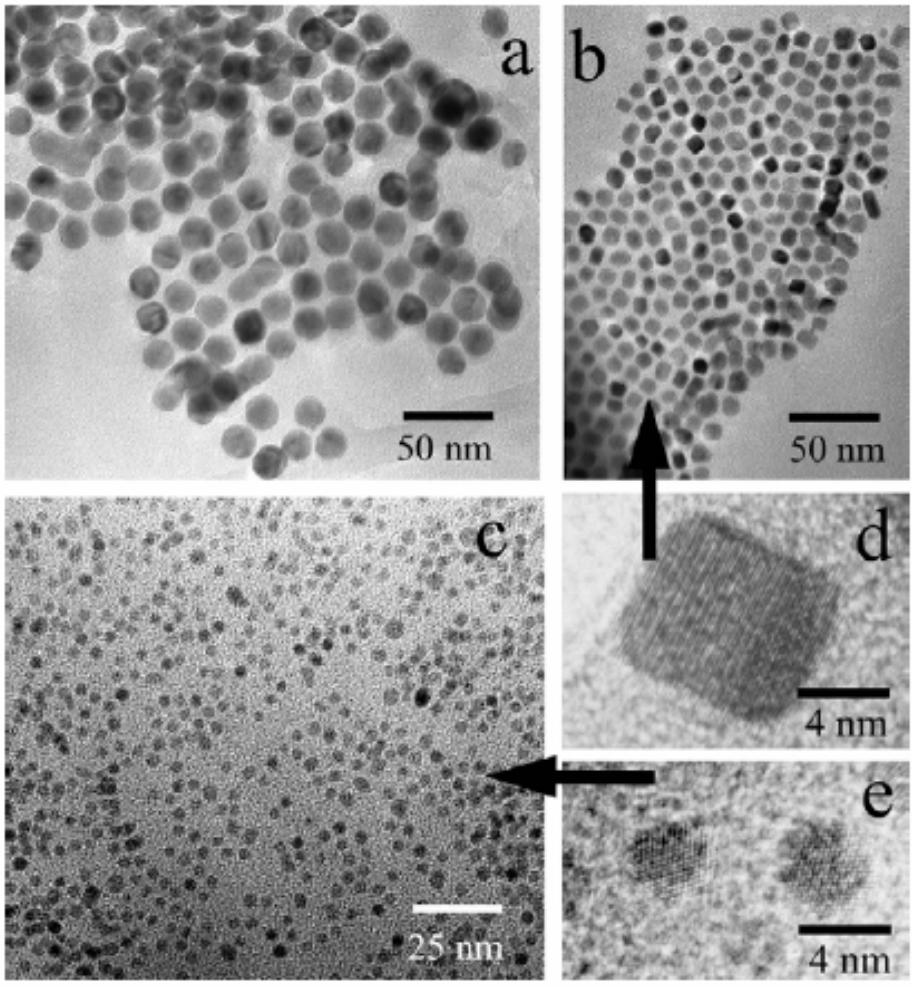

Figure 5.6 TEM images of salt-matrix-annealed fct FePt nanoparticles annealed at 700 °C for 2 hours. (a) 15 nm with NaCl:FePt ratio of 100 : 1, (b) 8 nm with the ratio of 40 : 1, (c) 4 nm with the ratio of 40 : 1, (d) and (e) are the high resolution TEM images for (b) and (c), respectively [70]

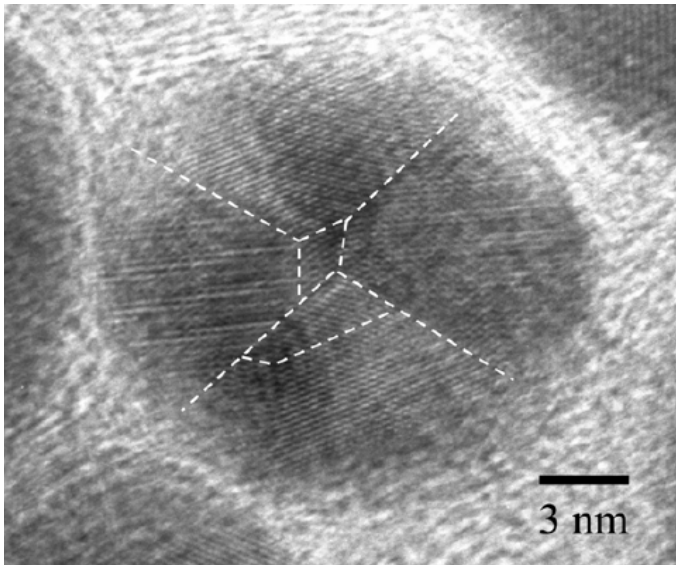

Figure 5.7 HRTEM image of an fct FePt nanoparticle annealed at 700 °C for 4 hours in salt-matrix, showing the polycrystalline morphology [70]

In order to maximize the fcc-to-fct conversion, the time of the salt-matrix annealing was extended from 2 hours to 4 hours at temperature of 700 ^{o}C. By adjusting to the proper NaCl:FePt ratio (discussed in 5.2.2 and 5.2.3), monodisperse fct FePt nanoparticles with diameters from 4 nm to 15 nm were obtained though 2 nm FePt nanoparticles with retained size did not convert to fct phase as discussed in 5.1.1. Figures 5.8 (a) to (e) show the TEM images of as-synthesized FePt nanoparticles with sizes from 2 nm to 15 nm. Figure 5.8 (e) shows the core-shell structure of 15 nm as-synthesized nanoparticles as described in previous discussions. Figure 5.8 (f) shows the TEM image of 2 nm unconverted FePt particles annealed at 700 ^{o}C for 8 hours and (g) to (j) show those of 4 to 15 nm fct FePt particles annealed at 700 ^{o}C for 4 hours. By comparing the TEM images of as-synthesized and annealed particles, we can conclude that the salt-matrix annealing technique has been applied to successfully produce monodisperse fct

phase FePt nanoparticles with retained sizes and shapes as starting as-synthesized nanoparticles in the annealing condition that completes the maximum atomic ordering, therefore the maximum converted fct phase. In the case of 2 nm FePt nanoparticles, even after being annealed in salt-matrix at 700 ^{o}C for 8 hours, the particle size was retained so that no fcc-to-fcc conversion was obtained as discussed in 5.1.1.

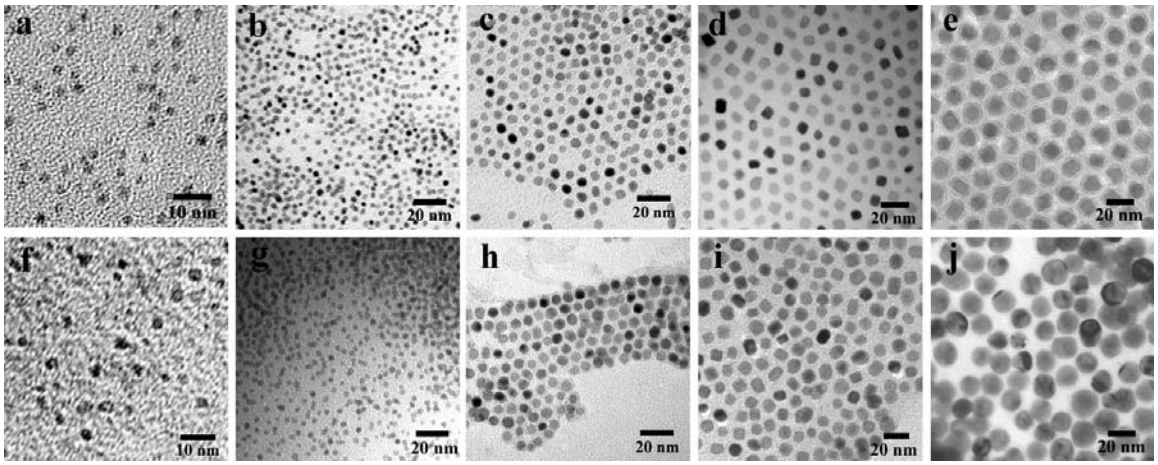

Figure 5.8 TEM images of as-synthesized FePt nanoparticles (a) 2 nm, (b) 4 nm, (c) 6 nm, (d) 8 nm, (e) 15 nm and FePt nanoparticles (f) 2 nm annealed at 700^{o}C for 8 hours, (g) 4 nm, (h) 6 nm, (i) 8 nm, (j) 15 nm annealed at 700^{o}C for 4 hours

5.2.2 NaCl:FePt Ratio Effect

The NaCl:FePt ratio in salt-matrix annealing technique has been adjusted from 1:1 to 400:1 to investigate the optimal experimental parameters. Figure 5.9 shows TEM images of the as-synthesized 15 nm FePt nanoparticles and the particles after being annealed at 700 ^{o}C for 2 hours with different NaCl:FePt ratios. For the ratio of 4:1, large particles as big as 50 nm can be found and the sample has a very wide size distribution because of sintering of particles during annealing. (see figure 5.9 (b)) When the ratio was increased to 40:1, the sintering was dramatically reduced except a few larger particles can

still be observed, as seen in figure 5.9 (c). Figure 5.9 (d) shows that when the ratio of 100:1 was used, the sintering was prevented completely and the particles size and shape were retained. It is proved that the higher the NaCl:FePt ratio is, the lesser the sintering occurs during annealing. In the case of the 15 nm FePt particles, when the ratio is lower than 40:1, monodisperse fct nanoparticles cannot be obtained from the heat treatment at 700 ^{o}C for 2 hours. When the annealing condition is fixed, lower salt ratios give significant particle sintering and agglomeration.

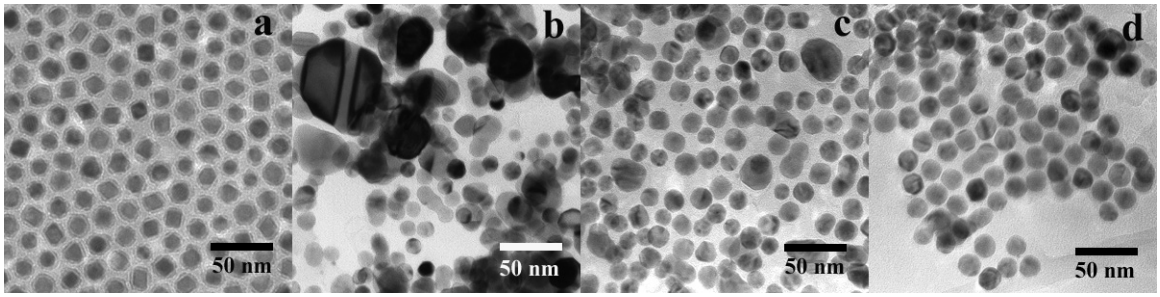

Figure 5.9 TEM images of 15 nm FePt nanoparticles (a) as-synthesized, and annealed in salt-matrix at 700 ^{o}C for 2 hours with NaCl:FePt ratios of (b) 4:1, (c) 40:1 and (d) 100:1

5.2.3 FePt Particle Size Effect

On the other hand, in salt-matrix annealing, the degree of sintering of particles is also related to the particle size of starting fcc FePt nanoparticles. Figure 5.10 shows the TEM images of 4 nm FePt nanoparticles annealed in different conditions with different NaCl:FePt ratios. Under the same annealing condition, 40:1 ratio was sufficient to prevent the sintering for 4 nm particles (figure 5.10 (a)) while sintering still occurred for 15 nm particles. This is related to the fact that particles with larger diameter have much larger spherical surface area, which results in higher probability to contact each other in

the NaCl matrix during the heat treatments. Therefore, for particles with larger diameter, higher salt ratios must be used to effectively separate particle from particle in the matrix during heat treatment and eventually prevent sintering and agglomeration.

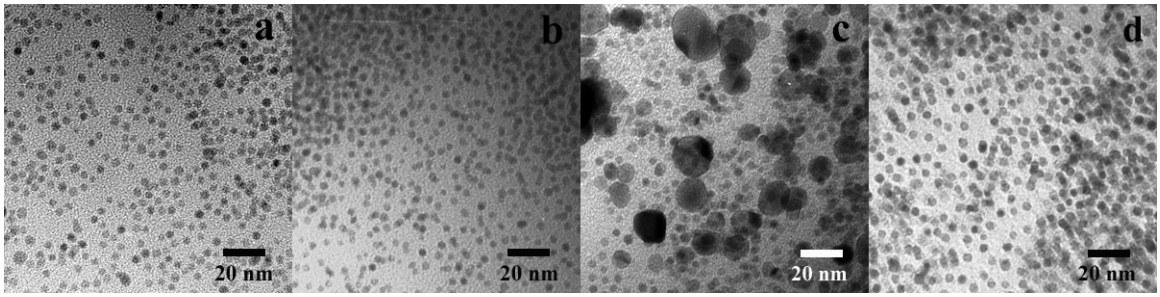

Figure 5.10 TEM images of 4 nm FePt nanoparticles annealed at (a) 700 ^{o}C for 2 hours with NaCl:FePt ratio of 40:1, (b) 700 ^{o}C for 4 hours with NaCl:FePt ratio of 100:1, (c) 700 ^{o}C for 8 hours with NaCl:FePt ratio of 100:1 and (d) 700 ^{o}C for 8 hours with NaCl:FePt ratio of 400:1

5.2.4 Annealing Condition Effect

In the study of 4 nm FePt nanoparticles, annealing time longer than 4 hours at 700 ^{o}C was tested. It has been found that both the annealing conditions and NaCl:FePt ratios have significant effects in preventing sintering of particles. As shown in figure 5.10 (b), when the NaCl:FePt ratio was increased from 40:1 to 100:1 and the annealing time was extended from 2 hours to 4 hours, monodisperse 4 nm FePt nanoparticles could still be obtained. However, the ratio of 100:1 was not sufficient to prevent sintering when the annealing time was increased to 8 hours. 4 nm nanoparticles sintered to form particles as large as 20 nm (see figure 5.10 (c)). When the ratio was continuously increased from 100:1 to 400:1, sintering of particles was successfully prevented again for annealing up to 8 hours, as shown in figure 5.10 (d). Thus, annealing at higher temperatures or extended

time should be accompanied with higher NaCl:FePt ratios to avoid sintering and obtain monodisperse nanoparticles.

5.3 Magnetic Properties of FePt Nanoparticles

Figure 5.11 shows the hysteresis loops of 2 nm FePt nanoparticles annealed in salt-matrix in different conditions, which were measured in AGM. Coercivity was not developed for all annealing conditions because 2 nm FePt nanoparticles did not convert to fct phase with magnetic anisotropy. On the other hand, significant coercivity was observed when FePt nanoparticles with sizes from 4 to 15 nm were converted to fct phase with high magnetic anisotropy. As shown in the hysteresis loops measured by SQUID in figure 5.12, for all particles with different sizes, coercivity increases with considerable values as the annealing temperature or time increases. When the annealing condition was 700 ^{o}C for 4 hours, the maximum coercivity values were obtained, which are 8 kOe, 23.3 kOe, 28.5 kOe and 16.7 kOe for 4 nm, 6 nm, 8 nm and 15 nm fct FePt nanoparticles, respectively.

Figure 5.13 shows the relation between the coercivity measured at room temperature and the particle diameter, which follows the same trend as the long-range ordering parameter as shown in figure 5.5. From 4 nm to 8 nm, coercivity increases when the particle diameter increases for each particular annealing condition, which may be related to the size-dependent chemical ordering of FePt nanoparticles. Larger nanoparticles with more developed chemical ordering have higher anisotropy, therefore, higher coercivity. [115] The relatively low coercivity of 15 nm fct FePt nanoparticles may be due to their polycrystalline morphology. As shown in the HRTEM image in

figure 5.7, the superposition of coercivities of crystal grains pointing to different directions results in lower sum of coercivity as a particle. As figures 5.5 and 5.13 demonstrate, both chemical ordering and magnetic anisotropy are particle-size-dependent for FePt nanoparticles, which leads to the size-dependent long-range ordering parameter and coercivity, respectively. Figure 5.14 shows the hysteresis loops of fct FePt nanoparticles measured at temperatures as low as 5 K. As temperature decreases from room temperature, the magnetic anisotropy of the nanoparticles increases, which results in increasing coercivity.

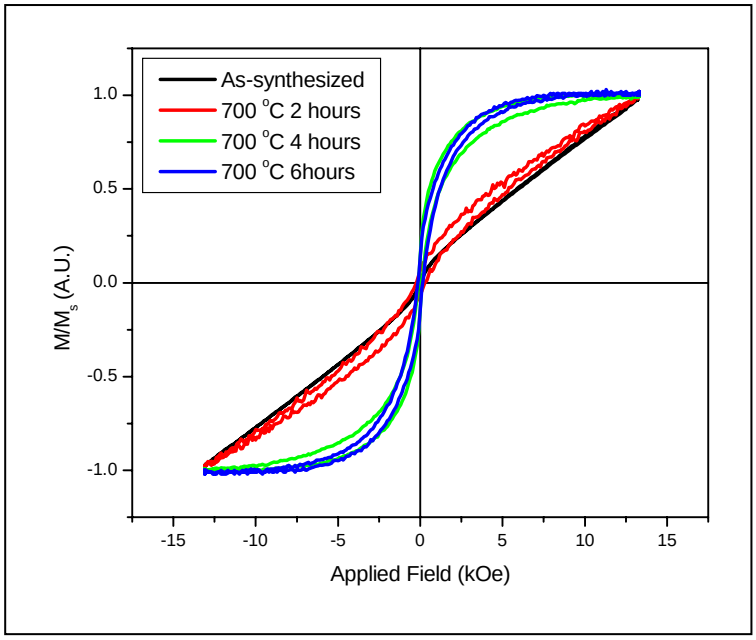

Figure 5.11 Hysteresis loops of 2 nm FePt nanoparticles annealed in salt-matrix in different conditions

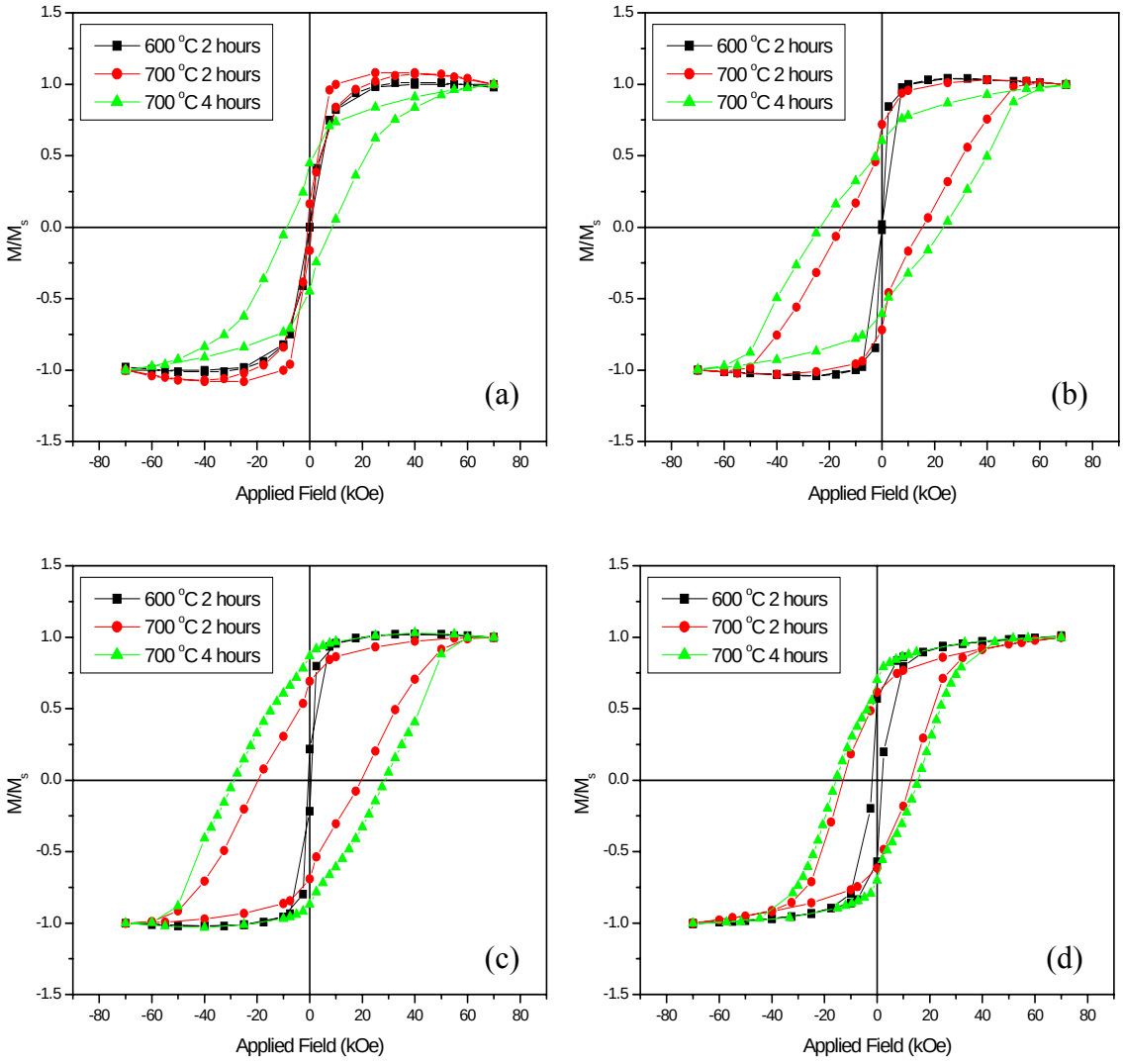

Figure 5.12 Hysteresis loops of FePt nanoparticles with diameters of (a) 4 nm, (b) 6 nm, (c) 8 nm and (d) 15 nm annealed in different conditions

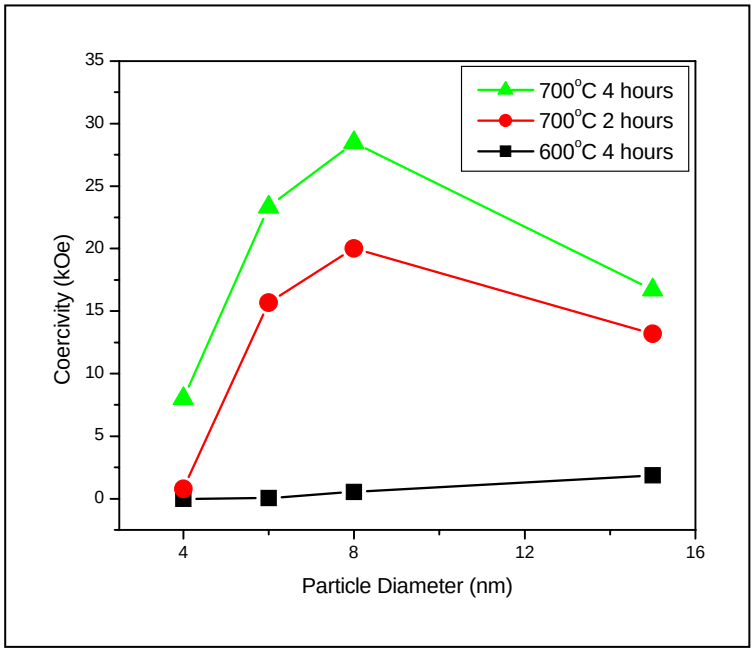

Figure 5.13 Coercivity vs. particle diameter under different annealing conditions

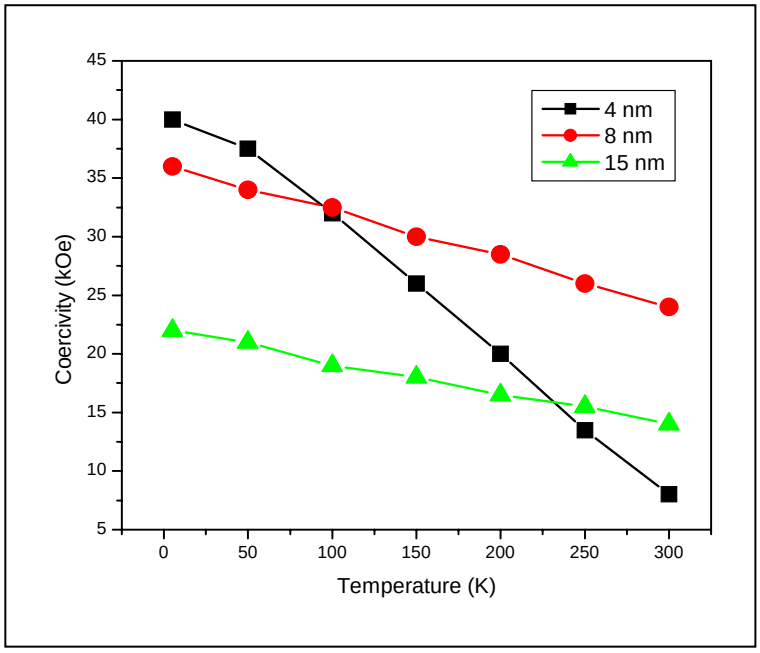

Figure 5.14 Coercivity vs. temperature for different particle sizes

Theoretically, fct FePt particles with magnetocrystalline anisotropy should be aligned under magnetic field and therefore, the aligned specimens could show different magnetization curves when being measured in different directions. Huge efforts have been made to produce anisotropic nanostructured assemblies in our experiment. The fct FePt nanoparticles were mixed in binders, such as epoxy or PVC, and put in a magnetic field as high as 29 T. The field was applied on the specimens until the liquid blinders were hardened so that nanoparticles would be aligned. However, no obvious difference was found in the magnetization curves measured in the parallel and perpendicular directions to the aligning field (figure 5.15).

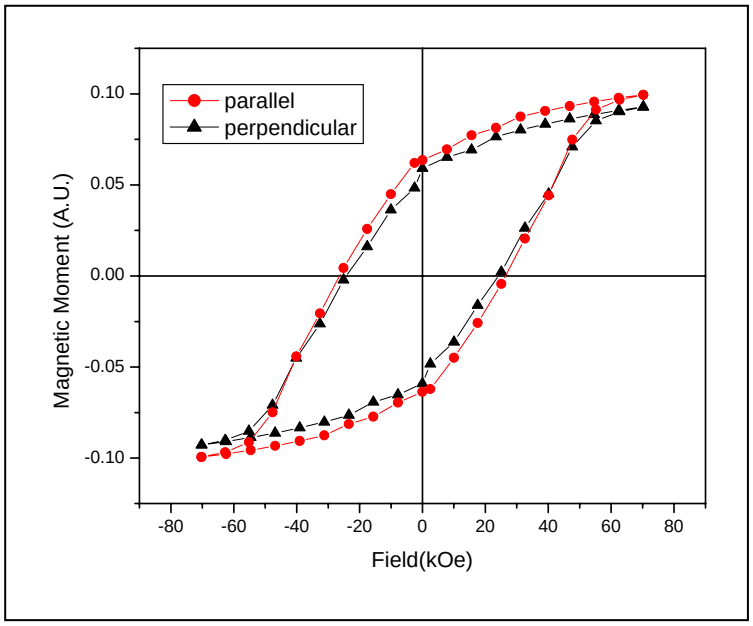

Figure 5.15 Hystersis loops of 8 nm fct FePt nanoparticles aligned under 29 T magnetic field mixed in epoxy

One possible reason for this failure of alignment is that each of the fct FePt nanoparticles is a small permanent magnet so that they attract each other to form large

aggregations, which makes the rotation of individual particles difficult. Besides the magnetic force, the chemical bonding among the surfaces of nanoparticles may also be the reason of the formation of large aggregations. Another possible reason may be that it is difficult to rotate the nanoparticles with very fine dimension in the epoxy binder because of the friction. This extremely high friction is caused by the high viscosity of epoxy and the huge surface area of the nanoparticles.

To reduce the friction, the fct FePt nanoparticles were aligned in low-viscosity binders, such as alcohol and water, under a magnetic field of 7 T in SQUID. The specimens were cooled down under the magnetic field, from room temperature at which alcohol and water are in liquid form, to temperatures below their freezing points, and the demagnetization curves were measured at these temperatures. These curves were then compared with the ones measured for the same specimens cooled without the magnetic field, which results in randomly oriented nanoparticles. Figure 5.16 shows the demagnetization curves measured from the aligned and random nanoparticles in frozen alcohol at temperature of 10 K. Significantly higher remanence and coercivity can be observed for the aligned nanoparticles though we were not able to saturate the magnetization under 7 T magnetic field at 10 K.

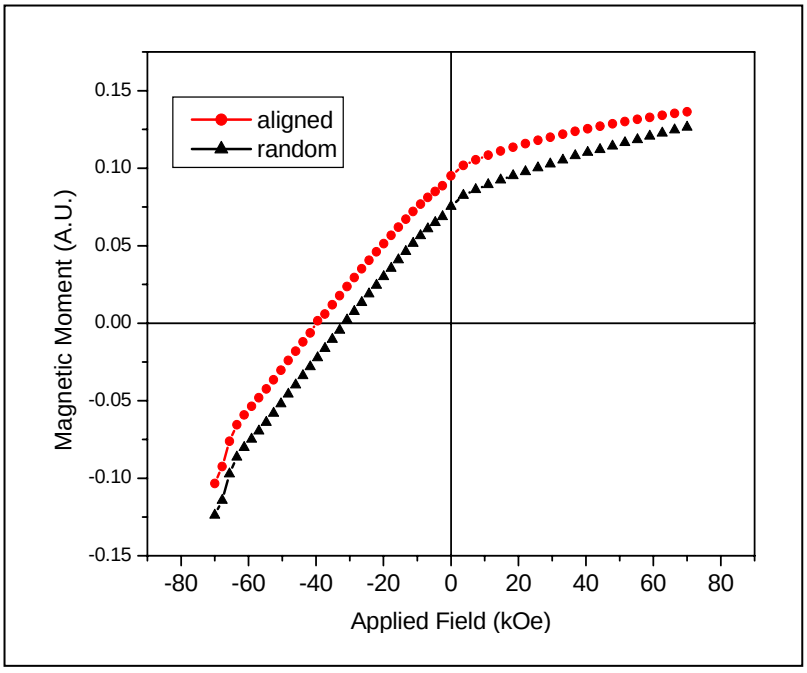

Figure 5.16 Demagnetization curves measured at 10 K from the aligned and random 8 nm fct FePt nanoparticles in frozen alcohol

Another reason for the difficulty in aligning the nanoparticles is associated with the polycrystalline feature of the annealed 15 nm fct FePt nanoparticles. Figure 5.7 shows an example of an annealed 15 nm FePt nanoparticle in a high resolution TEM image. The sample comprises of more than 50% of the plycrystalline particles, by a rough estimation. In the case of polycrystalline nanoparticles, the relationship between domains and grains can be very complicated and the magnetization reversal cannot be described in a simple model. Further study is needed for an extended understanding of this issue.

5.4 Magnetic Ordering of FePt Nanoparticles

The magnetic ordering of FePt nanoparticles was characterized by the temperature dependence of magnetization from which Curie temperature could be obtained. In this characterization carried out by a VSM, temperature was first brought from room temperature to a temperature as high as 1000 K and then decreased from high temperature back to room temperature so that loops of magnetic moment versus temperature could be recorded. Figure 5.17 shows the M-T loops for salt-matrix annealed FePt nanoparticles with diameters from 2 to 15 nm, which were measured with and without salt-matrix. As shown in the loops in figure 5.17, the magnetization of samples vanishes as the temperature increases above a critical point, which indicates that the magnetic ordering caused by ferromagnetism starts to disappear above a critical temperature, known as Curie temperature. Grain growth of nanoparticles occurred for samples measured without salt-matrix at high temperatures due to the absence of the protection of salt, which results in sintered bulk samples of FePt. On the other hand, the samples measured in salt-matrix could have retained nano-scaled particle sizes so that they represent the magnetic ordering behaviors of the FePt nanoparticles with different sizes. Obviously, the loops measured without salt-matrix that represent the FePt bulks have different behaviors from the ones measured with salt matrix that represent the FePt nanoparticles. As it can be observed, for a sample with particular particle size, magnetization vanishes at a lower temperature for the samples measured without salt-matrix than the ones measured with salt matrix. For 2 nm FePt nanoparticles, there is no

obvious drop of magnetization to a certain minimum point when it was measured with salt matrix, which is very different from the M-T loop measured without salt-matrix.

Curie temperature was determined by the intersection of the steepest tangents to the M-T loops as shown in figure 5.17. [116] The size-dependence of Curie temperature is demonstrated in figure 5.18. When the samples were measured in salt-matrix so that they were kept in nano-scale with desired particle sizes, Curie temperature increases as the particle size increases, as shown in the red curve of figure 5.18. This indicates that fct FePt nanoparticles with larger diameter have more stable magnetic ordering so that they need higher thermal energy to overcome the exchange interactions between magnetic moments, which results in higher Curie temperature. No Curie temperature could be determined from the M-T loop of 2 nm FePt nanoparticles measured with salt-matrix, which is due to the fact that they were not able to convert to fct hard-magnetic phase.

In the case of samples measured without salt, the Curie temperature was found to be obviously lower than the one measured with salt matrix, which implies that Curie temperature experienced significant decline as the nanoparticles turn to bulks. The reason for this phenomenon might be due to the nano-scale effect of particles. [104, 114] For nanoparticles, there is relatively larger fraction of atoms on the surface, which results in a different magnetic interaction behavior and therefore a different Curie temperature behavior. The Curie temperatures of samples measured without salt matrix do not follow the size-dependent behavior as perfectly as samples measured with salt matrix, which may be due to the different degree of sintering. In the case of 2 nm sample, Curie temperature could be determined because the sample sintered to form much larger grains

so that the fct transition could occur. The behavior of size-dependent Curie temperature can be also described in the curve of ΔT_c versus particle size in figure 5.19, where ΔT_c is the difference in T_c between samples for particular particle size measured with and without salt-matrix. ΔT_c increases as the particle size increases and the inconsistent behavior of 15 nm fct FePt nanoparticles may be caused by the difference in the degree of sintering as discussed above.

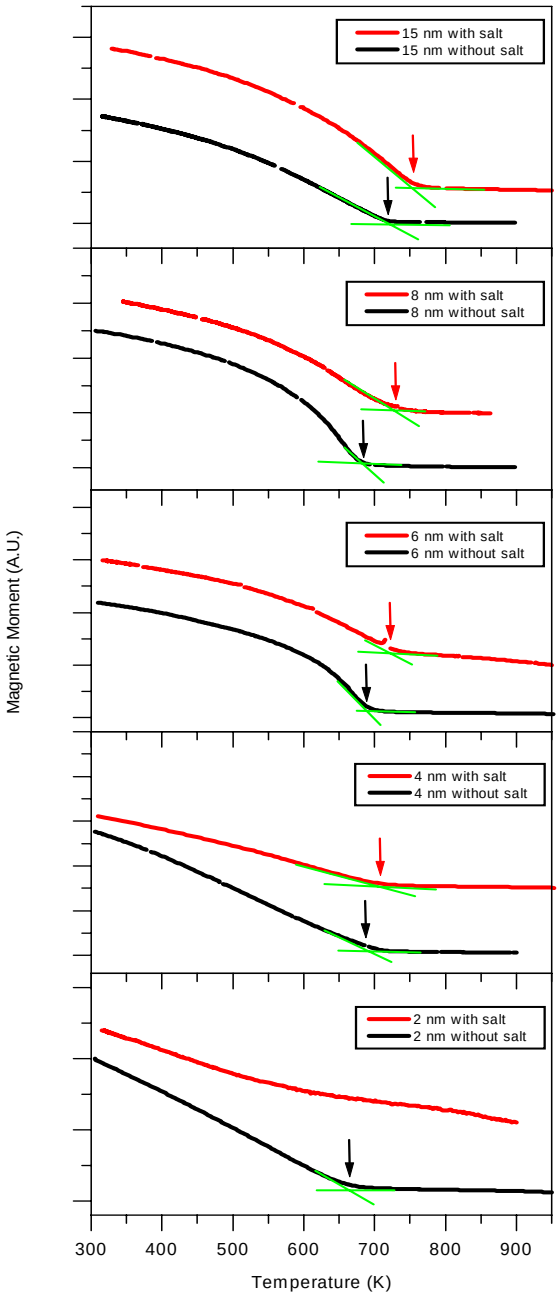

Figure 5.17 M-T loops of fct FePt nanoparticles with different sizes measured with and without salt matrix

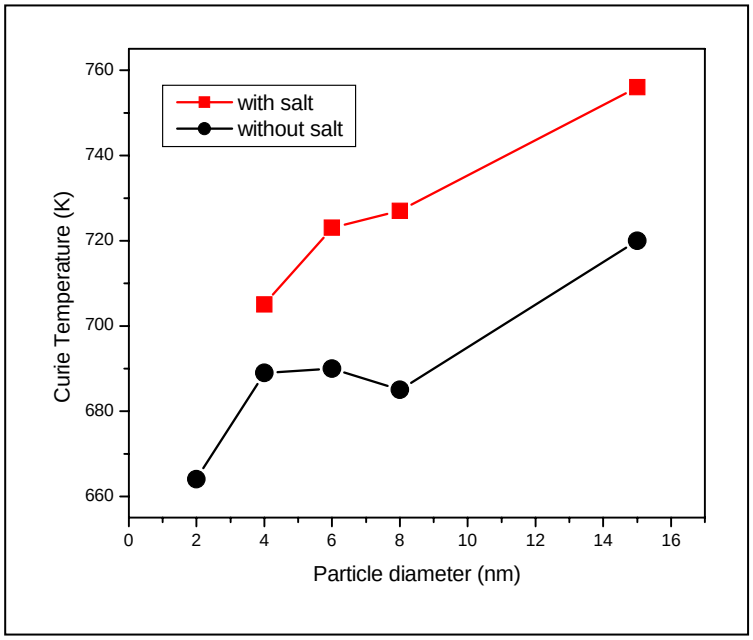

Figure 5.18 Curie temperature vs. particle diameter for samples measured with and without salt matrix

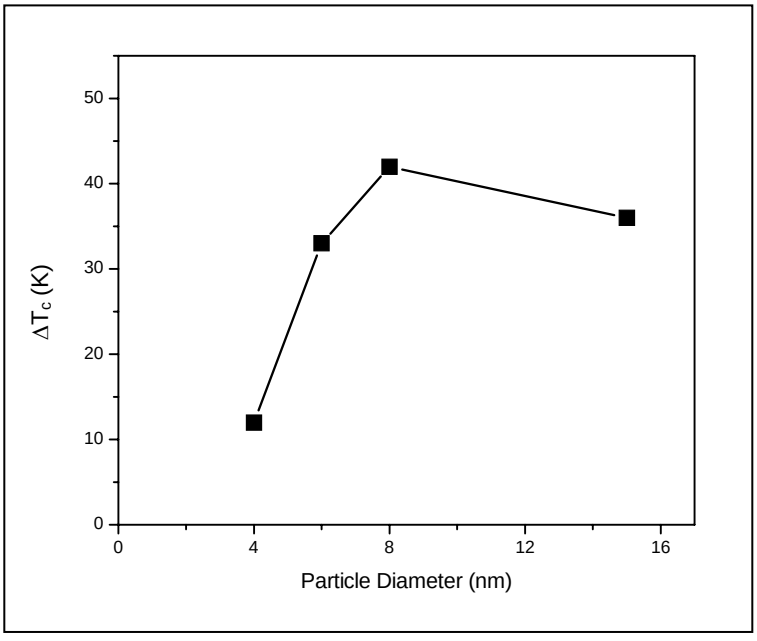

Figure 5.19 ΔT_c vs. particle diameter, where ΔT_c is the difference in T_c between samples measured with and without salt matrix

CHAPTER 6

SUMMARY

There are two major challenges for the applications of FePt nanoparticles. Firstly, the as-synthesized FePt nanoparticles are of face-centered cubic (fcc) phase, in which Fe and Pt atoms are positioned in atomic sites randomly. The FePt nanoparticles with the fcc structure do not have magnetic anisotropy that is necessary for tapplications of hard-magnetic nanoparticles. In order to make hard-magnetic nanoparticles with high magnetic anisotropy, fcc phase FePt nanoparticles must be converted to face-centered tetragonal (fct) phase. In the fct structure of FePt, Fe and Pt atoms occupy corresponding atomic sites orderly and periodically. Secondly, heat treatments that are required to convert FePt nanoparticles from fcc phase to fct phase cause sintering and agglomeration of nanoparticles. This phenomenon results in particles with irregular shapes and large size distribution, which is a great holdback of the applications of the hard-magnetic FePt nanoparticles.

Salt-matrix annealing technique was developed and applied as the solution to these two challenges. NaCl particles with size reduced by wet surfactant-assisted ball milling were introduced as the separating media during the heat treatments. FePt nanoparticles embedded in the salt-matrix do not contact each other so that sintering can be effectively prevented during heat treatments and fcc-to-fct transition is allowed to be completed at the same time. Monodisperse fct FePt nanoparticles with sizes varying from

2 to 15 nm have been successfully prepared by chemical method. After the salt-matrix annealing, the size and shape of the FePt nanoparticles were retained. The XRD analysis showed that the chemical ordering of FePt nanoparticles with diameters from 4 to 15 nm is most complete when the annealing condition is 700 ^{o}C for 4 hours. As the particle size increases, the long-range ordering parameter increases. The 15 nm FePt nanoparticles have a relatively low ordering parameter due to their polycrystalline structure. Magnetic hardening follows the same particle-size-dependent trend as the long-range ordering parameter. Coercivity as high as 30 kOe has been obtained for 8 nm fct FePt nanoparticles at room temperature. From the electron diffraction analysis, 2 nm FePt nanoparticles were found not to convert to fct ordered phase even after being annealed at 700 ^{o}C for 8 hours, because of their small particle size. Curie temperatures of the fct FePt nanoparticles were found to be size-dependent as well. Lager particle size results in higher Curie temperature. A decrease of Curie temperature was observed when the fct FePt nanoparticles were sintered during the M-T measurements. This phenomenon is very interesting and the reason for it still needs further study.

FePt hard-magnetic nanoparticles are one of the best candidates for many applications as mentioned in the previous chapters. This study helps us better understand the production technique of fct phase FePt nanoparticles and the size-effect on their characteristics. So far, the fct FePt nanoparticles produced in this study are the only available hard-magnetic nanoparticles at room temperature with particle size down to 4 nm. Moreover, these nanoparticles are monodisperse and free of non-magnetic impurities with controllable size and shape. However, with these fct FePt nanoparticles, extended

efforts should be made to produce anisotropic and high-energy-product nanocomposite assemblies and bulks, and to achieve the compatibility to biological systems for bio-applications.

APPENDIX A

UNITS OF MAGNETIC PROPERTIES

Table A.1 Units of magnetic properties [46]

Quantity	Symbol	Gaussian & cgs emu	Conversion factor, C [b]	SI & rationalized mks [c]
Magnetic flux density, magnetic induction	B	gauss (G) [d]	10^{-4}	tesla (T), Wb/m^2
Magnetic flux	M	maxwell (Mx), $G\theta cm^2$	10^{-8}	weber (Wb), volt second (Vθs)
Magnetic potential difference, mangetomotive force	U, F	gilbert (Gb)	$10/4\pi$	ampere (A)
Magnetic field strength, magnetizing force	H	oersted (Oe), [e] Gb/cm	$10^3/4\pi$	A/m [f]
(Volume) magnetization [g]	M	emu/cm^3 [h]	10^3	A/m
(Volume) magnetization	$4\pi M$	G	$10^3/4\pi$	A/m
Magnetic polarization, intensity of magnetization	J, I	emu/cm^3	$4\pi\times10^{-7}$	T, Wb/m^2 [i]
(Mass) magnetization	σ, M	emu/g	1 $4\pi\times10^{-7}$	$A\theta m^2/kg$ $Wb\theta m/kg$
Magnetic moment	m	emu, erg/G	10^{-3}	$A.m^2/kg$, joule per tesla (J/T)
Magnetic dipole moment	j	emu, erg/G	$4\pi\times10^{-10}$	$Wb\theta m$ [i]
(Volume) susceptibility	χ, κ	dimensionless, emu/cm^3	4π $(4\pi)^2\times10^{-7}$	dimensionless henry per meter (H/m), $Wb/(A\theta m)$
(Mass) susceptibility	χ_ρ, κ_ρ	cm^3/g, emu/g	$4\pi\times10^{-3}$ $(4\pi)^2\times10^{-10}$	M^3/kg $H\theta m^2/kg$
(Molar) susceptibility	χ_{mol}, κ_{mol}	cm^3/mol, emu/mol	$4\pi\times10^{-6}$ $(4\pi)^2\times10^{-13}$	m^3/mol $H\theta m^2/mol$
Permeability	μ	dimensionless	$4\pi\times10^{-7}$	H/m, $Wb/(A\theta m)$
Relative permeability [j]	μ_r	not defined		dimensionless
(Volume) evergy density, energy product [k]	W	erg/cm^3	10^{-1}	J/m^3
Demagnetization factor	D, N	dimensionless	$1/4\pi$	dimensionless

a. Gaussian units and cgs emu are the same for magnetic properties. The dfining relation is $B=H+4\pi$.
b. Multiply a number in Gaussian units by C to convert it to SI (e. g., $1\ G\times10^{-4}\ T/G=10^{-4}\ T$).
c. SI (Système International d' Unités) has been adopted by the National Bureau of Standards. Where two conversion factors are given, the upper one is recognized under, or consistent with, SI and is based on the definition $B=\mu_o(H+M)$, where $\mu_o=4\pi\times10^{-7}$ H/m. The lower one is not recognized under SI and is based on the definition $B=\mu_oH+J$, where the symbol I is often used in place of J.
d. 1 gauss=10^5 gamma (γ).
e. Both oersted and gauss are expressed as $cm^{-1/2}\theta g^{1/2}\theta s^{-1}$ in terms of base units.
f. *A/m* was often expressed as "ampere-turn per meter" when used for magnetic filed strength.
g. Magnetic moment per unit volume.
h. The designation "emu" is not a unit.
i. Recognized under SI, even though based on the definition $B=\mu_oH+J$. See footnote c.
j. $\mu_r=\mu/\mu_o=1+\chi$, all in SI. μ_r is equal to Gaussian μ.
k. $B\theta H$ and $\mu_oM\theta H$ have SI units J/m^3; MθH and $B\theta H/4\pi$ have Gaussian units erg/cm^3.

APPENDIX B

CRYSTRAL STRUCTURE OF FERRITE

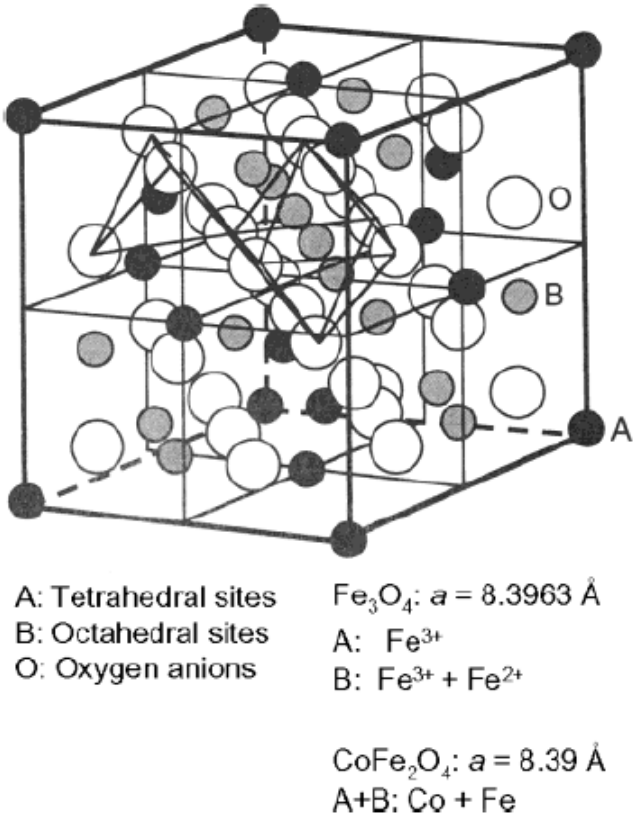

Figure B.1 Schematic model of the Spinel unite cell structure [56]

The spinel structure has two cation sites: the tetrahedrally coordinated A sites and the octahedrally coordinated B sites. For Fe_3O_4, the A and B positions are occupied by $Fe^{3+}$and Fe^{2+} cations, respectively. For $CoFe_2O_4$, the A and B positions are equally occupied by Co and Fe cations. Fe_3O_4 and $CoFe_2O_4$ have almost the same lattice parameters: a = 8.3963 Å for Fe_3O_4, a = 8.39 Å for $CoFe_2O_4$. The mass densities for Fe_3O_4 and $CoFe_2O_4$ are almost identical.

APPENDIX C

FePt PHASE DIAGRAM

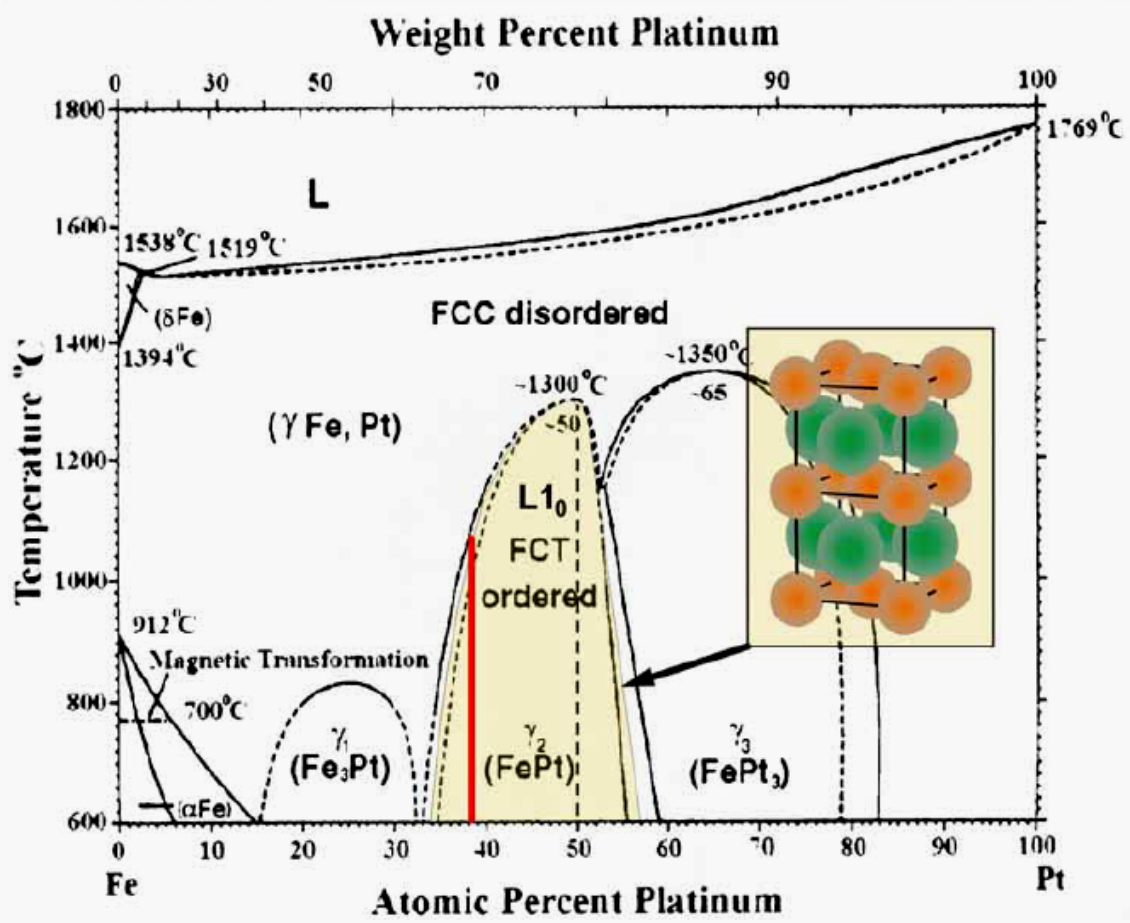

Figure C.1 FePt phase diagram and schematic representation of structure transformation between fcc and fct FePt. Orange circles represent Fe atoms and green circles represent Pt atoms in unit cells [117]

APPENDIX D

RESEARCH ACOMPLISHMENTS

Award

- Awarded "Scharff Award Scholarship" for research achievements on April 25, 2006 by the Department of Physics, University of Texas at Arlington.

Publications

- "Monodisperse face-centered tetragonal FePt nanoparticles with giant coercivity", Kevin Elkins, **Daren Li**, Narayan Poudyal, Vikas Nandwana, Zhiqiang Jin, Kanghua Chen and J. Ping Liu, *Journal of Physics D: Applied Physics,* **38,** 2306 (2005).

- "Hard magnetic FePt nanoparticles by salt-matrix annealing", **Daren Li**, Narayan Poudyal, Vikas Nandwana, Kevin Elkins, Zhiqiang Jin and J. Ping Liu, *Journal of Applied Physics*, **99**, 1 (2006) (in press).

- "Magnetic Properties of FePt Nanoparticles Annealed with NaCl", B. A. Jones, J. D. Dutson, K. O'Grady, B. J. Hickey, **Daren Li**, Narayan Poudyal and J. Ping Liu, *IEEE Transactions on Magnetics*, (to be published in October 2006).

Conference Presences

- Accepted abstract "Preparation of Monodisperse Fct FePt Nanoparticles", Kevin Elkins, **Daren Li**, J. Ping Liu, *American Physical Society March Meeting 2005*, March, 2005, Los Angeles, CA, USA.

- Accepted abstract and oral presentation "Hard Magnetic FePt Nanoparticles by Salt-matrix Annealing", **Daren Li**, Kevin Elkins, Narayan Poudyal, Vikas Nandwana, Zhiqiang Jin, Kanghua Chen and J. Ping Liu, *The 50th Conference on Magnetism and Magnetic Materials*, October, 2005, San Jose, CA, USA.

- Accepted abstract and oral presentation "Size Effect on Chemical Ordering in Face-Centered Tetragonal FePt Nanoparticles", **Daren Li**, Narayan Poudyal, Vikas Nandwana and J. Ping Liu, *American Physical Society March Meeting 2006*, March, 2006, Baltimore, MD, USA.

- Accepted abstract "Magnetism of Discrete $L1_0$ Ordered FePt Nanoparticles", Hao Zeng, Michael Demarco, **Daren Li**, and J. Ping Liu, *American Physical Society March Meeting 2006*, March, 2006, Baltimore, MD, USA.

- Accepted abstract "Magnetic Properties of FePt Nanoparticles Annealed with NaCl", B. A. Jones, J. D. Dutson, K. O'Grady, B. J. Hickey, **Daren Li**, Narayan Poudyal and J. Ping Liu, *IEEE International Magnetics Conference 2006*, May 2006, San Diego, CA, USA.

News Articles

- "Just Add Salt", titled news articles published in *Physics Web* in August 4, 2005. Link to the articles: http://physicsweb.org/articles/news/9/8/3/1.

- "For Nanoparticles, Just Add Salt", titled news articles published in *Nanotechweb.org*. Link to the articles: http://www.nanotechweb.org/articles/news/4/8/6/1.

- "Physicists Discover Table Salt is Solution to Creating the Smallest Magnets", titled news articles published in *UTA Today* in August 15, 2005.

REFERENCES

1. K. H. J. Buschow and De Boer F. R., "Physics of Magnetism and Magnetic Materials", Kluwer Academic/Plenum Publishers (2003).
2. S. Chikasumi, "Physics of Magnetism", John Wiley and Sons (1964).
3. B. D. Cullity, "Introduction to Magnetic Materials", Addison-Wesley Publishing (1972).
4. K. J. Klabunde, "Nanoscale Materials in Chemistry", John Wiley & Sons (2001).
5. A. P. Guimarães, "Magnetism and Magnetic Resonance in Solids", John Wiley & Sons (1998).
6. S. Nicola, "Magnetic Materials: Fundamentals and Device Applications", Cambridge University Press (2003).
7. Eric E. Fullerton, J. S. Jiang, S. D. Bader, "Hard/Soft Magnetic Heterostructures: Model Exchange-Spring Magnets", *Journal of Magnetism and Magnetic Materials*, **200**, 392 (1999).
8. http://www.azom.com/details.asp?ArticleID=637
9. E. F. Kneller, and R. Hawing "The Exchange-Spring Magnet: New Material for Permanent Magnets", IEEE Transactions on Magnetics, 27, 3588 (1991).

10. R. Coehoorn, D. B. de Mooij and C. de Waard "Meltspun Permanent Magnet Materials Containing Fe_3B as the Main Phase", *Journal of Magnetism and Magnetic Material*, **80**, 10 (1989).
11. R. Skomski, J.M.D. Coey, "Giant Energy Product in Nanostructured Two-Phase Magnets*", Physical Review B*, **48**, 15812 (1993).
12. R. Skomski and J. M. D. Coey, "Exchange Coupling and Energy Product in Random Two Phase Aligned Magnets", *IEEE Transactions on Magnetics*, **30**, 607 (1994).
13. D. Weller, A. Moser, L. Folks, M. E. Best, W. Lee, M. F. Toney, M. Schwckert, J. U. Thiele and M. F. Doerner, "High K_μ Materials Approach to 100 Gbits/in^2", *IEEE Transactions on Magnetics*, **36**, 10 (2000).
14. S. Sun, C. B. Murray, D. Weller, L. Folks and A. Moser, "Monodisperse FePt Nanoparticles and Ferromagnetic FePt Nanocrystal Superlattices", *Science,* **287,** 1989 (2000).
15. H. Zeng, J. Li, J. P. Liu, Z. L. Wang, and S. Sun, "Exchange-Coupled Nanocomposite Magnets by Nanoparticles Self-Assembly" *Nature*, **420**, 395 (2002).
16. Q. A. Pankhurst, J. Connolly J, S. K. Jones and J. Dobson J, "Applications of Magnetic Nanoparticles in Biomedicine", *Journal of Physics D: Applied Physics*, **36,** R167 (2003).
17. Kevin E. Elkins , Tejaswi S. Vedantam, J. P. Liu, Hao Zeng, Shouheng Sun, Y Ding, and Z. L. Wang, "Ultrafine FePt Nanoparticles Prepared by the Chemical Reduction Method", *Nano Letter*, **3,** 1647 (2003).

18. M. Chen, J. P. Liu, and S. Sun, "One-Step Synthesis of FePt Nanoparticles with Tunable Size**",** Journal *of American Chimerical Society,* **126**, 8394 (2004).

19. X. Teng and H. Yang "Synthesis of Face-Centered Tetragonal FePt Nanoparticles and Granular Films from Pt@Fe_2O_3 Core-Shell Nanoparticles", *Journal of American Chemical Society,* **125,** 14559 (2003).

20. O. Kitakami, Y. Shimada, K. Oikawa, H. Daimon and K. Fukamichi, "Low-Temperature Ordering of $L1_0$-CoPt Thin Films Promoted by Sn, Pb, Sb, and Bi Additives", *Applied Physics Letter*, **78**, 1104 (2001).

21. T. Maeda, T. Kai, A. Kikitsu, T. Nagase and J. Akiyama, "Reduction of ordering temperature of an FePt-ordered alloy by addition of Cu", *Applied Physics Letter*, **80**, 2147 (2002).

22. S. Kang, J. W. Harrell and D. E. Nikles , "Reduction of the fcc to L10 Ordering Temperature for Self-Assembled FePt Nanoparticles Containing Ag", *Nano Letter*, **2**, 1033 (2002).

23. S. S. Kang, D. E. Nickles and W. J. Harrell, "Synthesis, Chemical Ordering, and Magnetic Properties of Self-Assembled FePt–Ag Nanoparticle", *Journal of Applied Physics***, 93,** 7178 (2003).

24. X. Sun, S. Kang, J. W. Harrell, D. E. Nikles, Z. R. Dai, J. Li, and Z. L. Wang, "Synthesis, Chemical Ordering, and Magnetic Properties of FePtCu Nanoparticle Films", *Journal of Applied Physics*, **93**, 7337 (2003).

25. C. L. Platt, K. W. Wierman, E. B. Svedberg, R. van de Veerdonk, J. K. Howard, A. G. Roy and D. E. Laughlin, "L–1_0 Ordering and Microstructure of FePt Thin Films with Cu, Ag, and Au Additives", *Journal of Applied Physics*, **92**, 6104 (2002).

26. B. Jeyadevan, A. Hobo, K. Urakawa, C. N. Chinnasamy, K. Shinoda, and K. Tohji, "Towards Direct Synthesis of fct-FePt Nanoparticles by Chemical Route", *Journal of Applied Physics*, **93**, 7574 (2003).

27. B. Jeyadevan, K. Urakawa, A. Hobo, N. Chinnasamy, K. Shinoda, K. Tohji, David D. Julianto Djayaprawira, M.Tsunoda and M.Takahashi, "Direct Synthesis of fct-FePt Nanoparticles by Chemical Route", *Japanese Journal of Applied Physics*, **42**, 350 (2003)

28. K. Sato, B. Jeyadevan and K. Tojhi, *Journal of Magnetism and Magnetic Materials,* **266**, 227 (2003).

29. S. Kang, Z. Jia , S. Shi , D. E. Nikles and J. W. Harrell , "Easy Axis Alignment of Chemically Partially Ordered FePt Nanoparticles", *Applied Physics Letter*, **86**, 62503 (2005).

30. Y. Ding, S. A. Majetich, J. Kim, K. Barmak, H. Rollins and P. Sides, "Sintering Prevention and Phase Transformation of FePt Nanoparticles", *Journal of. Magnetism and Magnetic Materials,* **284**, 336 (2004).

31. M. Mizuno, Y. Sasaki, A. C. C. Yu and M. Inoue "Prevention of Nanoparticle Coalescence under High-Temperature Annealing", *Langmuir,* **20**, 11305 (2004).

32. H. Zeng, S. Sun, R. L. Sandstrom and C.B. Murray, "Chemical Ordering of FePt Nanoparticle Self-Assemblies by Rapid Thermal Annealing**",** *Journal of. Magnetism and Magnetic Materials,* **266,** 227 (2003).

33. S. Saita and S. Maenosono, "Chemical Ordering of FePt Nanoparticles by Pulsed Laser Annealing", *Journal of Physics: Condensed Matter,* **16,** 6385 (2004).

34. J. Lyubina, O. Gutfleisch, K. H. Muller and L. Schultz, "Structure and Hysteresis Properties of Nanocrystalline FePt Powders", *Journal of Magnetism and Magnetic Materials*, **290-291**, 547 (2005).

35. Y. Zhang, J. Wan, V. Skumryev, S. Stoyanov, Y. Huang, G. C. Hadjipanayis and D. Weller, "Microstructural Characterization of $L1_0$ FePt/MgO Nanoparticles with Perpendicular Anisotropy", *Applied Physics Letters*, **85**, 5343 (2004).

36. V. Nandwana, K. E. Elkins and J. P. Liu, "Magnetic Hardening in Ultrafine FePt Nanoparticle Assembled Films", *Nanotechnology*, **16,** 2823 (2005).

37. S. Yamamoto, Y. Morimoto, T. Ono and M. Takano, "Magneticaly Superior and Easy to Handle $L1_0$-FePt Nanoctrystals", *Apllied Pysics Letters*, **87**, 032503 (2005).

38. M. Aslam, L. Fu, S. Li and V. P. Dravid, "Silica Encapsulation and Magnetic Properties of FePt Nanoparticles", *Journal of Colloid and Interface Science*, **290**, 444 (2005).

39. Catherine C. Berry and Adam S. G. Curtis, "Fictionalization of Magnetic Nanoparticles for Application in Biomedicine", *Journal of Physics D: Applied Physics*, **36**, R198 (2003).

40. Taeghwan Hyeon, "Chemical Synthesis of Magnetic Nanoparticles", *Chemical Communication,* 927 (2003).

41. Adam Curtis, "Biomedical Aspects of Magnetic Nanoparticles", *Euro physics News*, **34**, 6 (2003).

42. M. Chastellainl, A. Petril, M. Hofmann and H. Hofmann, "Synthesis and Patterning of Magnetic Nanostructures", *European Cells and Materials*, **3**, 11 (2002).

43. D. K. Kim W. Voit, W. Zapka, B. Bjelke, M. Muhammed, and K.V. Rao, "*Material Research Society Symp. Proc*." **676** Y8. 32.1 (2001).

44. M. A. Willard, L.K. Kulrihara, E.E. Carpenter, S. Calvin and V.G. Harris, "Chemically Prepared Magnetic Nanoparticles", *International Material Reviews*, **49**, 3 (2004).

45. L. Fu, V.P. Dravid, K. Klug, X. Liu and C.A. Mirkin, " Synthesis and Patterning of Magnetic Nanostructures", *European Cell and Materials, 3 Suppl.* 2, 156 (2002).

46. R. B. Goldfarb and F.R., U.S. Department of Commerce, National Bureau of Standards, Boulder, Colorado 80303, March 1985. NBS Special Publication 696. For sale by the Superintendent of Documents, U.S. Government Printing Office, Washington, DC (2004).

47. C. A. Ross, "Patterned Magnetic Recording Media", *Annual Review of Material Research*, **31**, 203 (2001).

48. S. Okamoto, O. Kitkami, N. Kickuchi, T. Miyazaki, and Y. Shimada, "Size Dependences of Magnetic Properties and Switching Behavior in FePt $L1_0$ Nanoparticles", *Physical Review B*, **67**, 094422 (2003).

49. D. Weller, M. F. Doerner, "Extremely High-Density Longitudinal Magnetic Recording Media" *Annual Review of Materials Science*, **30**, 611 (2000).

50. Y. Shi, J. Ding and H. Yin, "$CoFe_2O_4$ Nanoparticles by the Mechanochemical Method", *Journal of Alloys and Compounds*, **303**, 290 (2002).

51. Yeong II Kim, Don Kim, and Choong Sub Lee, "Synthesis and Characterization of $CoFe_2O_4$ Magnetic Nanoparticles Prepared by Temperature-Controlled Co-Precipitation Method", *Physica B*, **337**, 42 (2003).

52. C. N. Chinnasamy, M. Senoue, B. Jeyadevan, Oscar Perales-Perez, K. Shinoda, and K. Tohji, " Synthesis of Size-Controlled Cobalt Ferrite Particles with High Coercivity and Squareness Ratio", *Journal of colloid and interface science*, **263**, 80 (2003).

53. http://www.carolina.com/physics/aboutferro.asp.

54. Hao Zeng, Shouheng Sun, J. Li and Z. L. Wang, and J. P. Liu, "Tailoring Magnetic Properties of Core/Shell Nanoparticles", *Applied Physics Letters*, **85**, 792 (2004).

55. Christy R, Vestal and Z. John Zhang, "Magnetic Spinel Ferrite Nanoparticles from Microemulsions" *International Journal of Nanotechnology*", **1**, 1/2 (2004).

56. Jing Li, Hao Zeng, Shouheng Sun, J. Ping Liu, and Zhong Lin Wang **, "**Analyzing the Structure of CoFe-Fe_3O_4 Core-Shell Nanoparticles by Electron Imaging and Diffraction", *Journal of Physical Chemistry B***, 108***,* 14005 (2004).

57. Yeong II Kim, Don Kim, and Choong Sub Lee, "Synthesis and Characterization of $CoFe_2O_4$ Magnetic Nanoparticles Prepared by Temperature-Controlled Co-Precipitation Method", *Physica B*, **337**, 42 (2003).

58. C. N. Chinnasamy, M. Senoue, B. Jeyadevan, Oscar Perales-Perez, K. Shinoda, and K. Tohji, " Synthesis of Size-Controlled Cobalt Ferrite Particles with High Coercivity and Squareness ratio", *Journal of Colloid and Interface Science*, **263**, 80 (2003).

59. M. Rajendran, R. C. Pullar, A. K. Bhattacharya, D. Das, S. N. Chintalapudi and C. K. Majumdar, "Magnetic Properties of Nanocrystalline $CoFe_2O_4$ Powders Prepared at Room Temperature: Variation with Crystallite Size", *Journal of Magnetism and Magnetic Materials,* **232**, 71 (2001).

60. P.C. Morais, V.K. Garg , A.C. Oliveira, L.P. Silva, R.B. Azevedo, A.M.L. Silva, E.C.D. Lima, " Synthesis and Characterization of Size-Controlled Cobalt-Ferrite-Based Ionic Ferrofluids", *Journal of Magnetism and Magnetic Materials,* **225** , 37 (2001).

61. N. Moumen, P. Veillet and M. P. Pileni, "Controlled Preparation of Nanosize Cobalt Ferrite Magnetic Particles", *Journal of Magnetism and Magnetic Materials*, **149**, 67 (1995).

62. Chao Liu, Bingsuo Zou, Adam J. Rondinone, and Z. John Zhang "Chemical Control of Superparamagnetic Properties of Magnesium and Cobalt Spinel Ferrite Nanoparticles through Atomic Level Magnetic Couplings", *Journal of American Chemical Society*, **122**, 6263 (2000).

63. Shouheng Sun, Hao Zeng, David B. Robinson, Simone Raoux, Philip M. Rice, Shan X. Wang, and Guanxiong Li, "Monodisperse MFe_2O_4 (M = Fe, Co, Mn) Nanoparticles", *Journal of Applied Chemical Society*, **126**, 273 (2004).

64. Shouheng Sun, and Hao Zeng, "Size-Controlled Synthesis of Magnetite Nanoparticles", *Journal of Applied Chemical Society*, **124**, 8204 (2002).

65. M. A. Willard, L.K. Kulrihara, E.E. Carpenter, S. Calvin and V.G. Harris, "Chemically prepared magnetic nanoparticles", *International Material Reviews*, **49**, 3 (2004).

66. T. Yogi and T. A. Nguyen, **"**Ultra High Density Media: Gigabit and Beyond", *IEEE Transactions on Magnetics*, **29**, 307 (1993).

67. J. Li, M. Mirzamaani, X. Bian, M. Doerner, D. Duan, K. Tang, M. Toney, T. Arnoldussen and M. Madison, "10 Gbit/in.^{2} Longitudinal Media on A Glass Substrate", *Journal of Applied Physics*, **85**, 4286 (1999).

68. V. V. Yakovlev, V. Lazarov, J. Reynolds, and M. Gajdardziska-Josifovska, "Laser-Induced Phase Transformations in Semiconductor Quantum Dots", *Applied Physics Letters*, **76**, 2050 (2000).

69. S. Sun, Eric E. Fullerton, D. Weller and C. B. Murray, " Compositionally Controlled FePt Nanoparticle Materials", *IEEE Transactions on Magnetics*, **37**, 1239 (2001).

70. K. Elkins, D. Li, N. Poudyal, V. Nandwana, Z. Jin, K. Chen and J. P. Liu, "Monodisperse Face-Centered Tetragonal FePt nanoparticles with Giant Coercivity", *Journal of Physics D: Applied Physics,* **38**, 2306 (2005).

71. B. Jeyadevan, A. Hobo, K. Urakawa, C. N. Chinnasamy, K. Shinoda, and K. Tohji, "Towards Direct Synthesis of fct-FePt Nanoparticles by Chemical Route", *Journal of Applied Physics*, **93** 7574 (2003).

72. S. Stavroyiannis, I. Panagiotopoulos, D. Niarchos, J. A. Christodoulides, Y. Zhang and G. C. Hadjipanayis, "CoPt/Ag Nanocomposites for High Density Recroding Media", *Applied Physics Letters*, **73**, 3453 (1998).

73. J. S. Miller and M. Drillon, "Magnetism: Molecules to Materials III", Wiley-Vch (2002).

74. R. Skomsky and J. M. Coey, "Giant Energy Product in Nanostructured Two-Phase Magnets", *Physical Review B*, **48**, 15812 (1993).

75. E. F. Kneller and R. Hawing, "The Exchange-Spring Magnet: A New Material Principle for Permanent Magnets", *IEEE Transactions on Magnetics*, **27**, 3588 (1991).

76. F. C. Meldrum, B. R. Heywood and S. Mann, "Magnetoferritin: In Vitro Synthesis of A Novel Magnetic Protein", *Science*, **257**, 522 (1992).

77. http://www.zarm.uni-bremen.de/2forschung/ferro/basic_info/applic/index.htm.

78. T. Pannaparayil and S.Komarneni, "Synthesis and Characterization of Ultra Fine Cobalt Ferrites", *IEEE Transactions on Magnetics*, **25**, 5 (1989).

79. Y. Ahn, E. J. Choi, S. Kim , H. N. Ok , "Magnetization and Mössbauer Study of Cobalt Ferrite Particles from Nanophase Cobalt Iron Carbonate", *Materials Letters,* **50** , 47 (2001).

80. V. Pillai, and D.O. Shah, " Synthesis of High-Coercivity Cobalt Ferrite Particles Using Water-in-Oil Microemulsions", Journal *of Magnetism and Magnetic Materials*, **163**, 243 (1996).

81. R. Vijayakumar, Yu Koltypin, I. Felner, A. Gedanken, "Sonochemical Synthesis and Characterization of Pure Nanometer-Sized Fe_3O_4 Particles", *Material Science and Engineering A*, **286**, 101 (2000).

82. W. D. Ristenpart, I. A. Aksay, and D. A. Saville, "Assembly of Colloidal Aggregates by Electro-Hydrodynamic Flow: Kinetic Experiments", *Physical Review E,* **69**, 021405 (2004).

83. G. F. Goya, "Handling the Particles Size and Distribution of Fe_3O_4 Nanoparticles through Ball Milling", *Solid State Communications*, **130**, 783 (2004).

84. S. Bid, A. Banerjee, S. Kumar, S. K. Pradhan, Udaya De, D. Banerjee, " Nanophase Iron Oxides by Ball-Mill Grinding and Their Mössbauer Characterization", *Journal of Alloys and Compounds*, **326**, 292 (2001).

85. K. V. P. M. Shafi, A. Gedanken, R. Prozorov and J. Balohgh, "Sonochemical Preparation and Size-Dependent Properties of Nanostructured $CoFe_2O_4$ Particles", *Chemical Material*, **10**, 3445 (1998).

86. J. G. Lee, J. Y. Park, C. S. Kin, "Growth of Ultra-Fine Cobalt Ferrite Particles by A Sol-Gel Method and Their Magnetic Properties" *Journal of Material Science*, **33**, 3965 (1998).

87. T. Sugimota, Y. Shimotsuma and H. Itoh, " Synthesis of Uniform Cobalt Ferrite Particles from a Highly Condensed Suspension of β-FeOOH and β-$Co(OH)_2$ Particles", *Power Technology*, **96**, 85 (1998).

88. F. Bensebaa, F. Zavaliche, P. L. Ecuyer, R.W. Cochrane, T. Veres, " Microwave Synthesis and Characterization of Co-Ferrite Nanoparticles", *Journal of Colliod and Interface Science*, **277**, 104 (2004).

89. Riki Hrpensess and Ahron Gedanken, "The Microwave-Assited Polyol Synthesis of Nanosized Hard Magnetic Material, FePt", *Journal of Material Chemistry,* **15**, 698 (2005).

90. W. Liu and P.G. McCormick, "Synthesis of Sm_2Co_{17} Alloy Nanoparticles by Mechanical Processing", *Journal of magnetism and magnetic materials*, **195**, L297 (1999).

91. X. Li and C. Kutal, "Synthesis and Characterization of Superparamagnetic $Co_xFe_{3-x}O_4$ Nanoparticles", *Journal of Alloys and Compounds*, **349**, 264 (2003).

92. G. B. Ji, S.L. Tang, S.K. Ren, F.M. Zhang, B.X. Gu, Y.W. Du, "Simplified Synthesis of Single-Crystalline Magnetic $CoFe_2O_4$ Nanorods by a Surfactant-Assisted Hydrothermal Process", *Journal of Crystal Growth*, **270**, 156 (2004).

93. Warren, B. E., *X-Ray Diffraction,* Dover, New York (1990).

94. Cullity, B. D., Elements of *X-ray Diffraction*, Addison-Wesley, London (1956).

95. A. Cebollada, D. Weller, J. Sticht, G. R. Harp, R. F. C. Farrow, R. F. Marks, R. Savoy, and J. C. Scott, "Enhanced Magneto-Optical Kerr Effect in Spontaneously Ordered FePt Alloys Quantitative Agreement between Theory and Experiment", *Physical Review Letters B*, **50**, 3419-3422 (1994).

96. J. A. Christodoulides, P. Farber, M. Daniil, H. Okaumura, G. C. Hadjipanayis, V. Skymryev, A. Simopoulos, and D. Weller, "Magnetic, Structural and Microstructural Properties of FePt/M (M=C, BN) Granular Films", *IEEE Transactions on Magnetics*, **37**, 1292 (2001).

97. J. M. Cowley, *Diffraction Physics*, Elsevier, Amsterdam, 231 (1995).

98. R. V. Petrova, R. R. Vanfleet, D. Richadson, B. Yao and K. R. Coffey, "Characterization of individual $L1_0$ FePt nanoparticles", *IEEE Transactions on Magnetics*, **41**, 3202 (2005).

99. K. Sato, Y. Hirotsu, H. Mori, Z. Wang and T. J. Hirayama, "Determination of Order Parameter of $L1_0$-FePd Nanoparticles by Electron Diffraction", *Journal of Applied Physics*, **97**, 084301 (2005).

100. K. Sato, Y. Hirotsu, H. Mori, Z. Wang, and T. Hirayama, "Long-Range Order Parameter of Single $L1_0$-FePd Nanoparticles Determination by Nanobeam Electron Diffraction: Particle Size Dependence of the Order Parameter", *Journal of Applied Physics*, **98**, 024308 (2005).

101. N. W. Ashcroft and N. D. Mermin, *Solid State Physics*, Saunders College Publishing (1976).

102. P. Heller and G. b. Benedek, "Nuclear Magnetic Resonance in MnF_2 Near the Critical Point", *Physical Review Letters*, **8**, 428 (1962).

103. J. E. Noackes, N. E. Tornberg and A. Arrott, "Initial Susceptibility of Iron and Iron Alloys Just Above Their Curie Temperatures", *Journal of Applied Physics*, **37**, 1264 (1966).

104. J. P. Chen, C. M. Sorensen, K. J. Klabunde, G. C. Hadjipanayis, E. devlin and A. Kostikas, "Size-Dependent Magnetic Properties of $MnFe_2O_4$ Fine Particles Synthesized by Coprecipitation", *Physical Review Letters B*, **54**, 9288 (1996).

105. L. Liao, J. C. Li, D. F. Wang, C. Liu, M. Z. Peng and J. M. Zhou, "Size Dependence of Curie Temperature in Co^+ Ion Implanted ZnO Nanowires", *Nanotechnology*, **17**, 830 (2006).

106. J. A. Christodoulides, M. J. Bonder, Y. Huang, Y. Zhang, S. Stoyanov, G. C. Hadjipanayis, A. Simopoulos and D. Weller, "Intrinsic and Hysteresis Properties of FePt Nanoparticles", *Physical Review Letters B*, **68**, 054428 (2003).

107. S. Okamoto, N. Kikuchi, O. Kitakami, T. Miyazaki, Y. Shimada and K. Fukamichi, "Chemical-Order-Dependent Magnetic Anisotropy and Exchange Stiffness Constant of FePt (001) Epitaxial Films", *Physical Review Letters B*, **66**, 024413 (2002).

108. T. S. Vedantam, J. P. Liu, H. Zeng and S. Sun, "Thermal Stability of Self-Assembled FePt Nanoparticles", *Journal of Applied Physics*, **93**, 7184 (2002).

109. Y. K. Takahashi, T. Koyama, M. Ohnuma, T. Ohkubo and K. Hono, "Size Dependence of Ordering in FePt Nanoparticles", *Journal of Applied Physics,* **95**, 2690 (2004).

110. Y. K. Takahashi, T. Ohkubo, M. Ohnuma and K. Hono, "Size Effect on the Ordering of FePt Granular Films", *Journal Applied Physics,* **93**, 7166 (2003).

111. T. Miyazaki, O. Kitakami, S. Okamoto, Y. Shimada, Z. Akase, Y. Murakami, D. Shindo, Y. K. Takahashi and K. Hono, "Size Effect on the Ordering of L10 FePt Nanoparticles", *Physical Review Letters B*, **72**, 144419 (2005).

112. B. Yang, M. asta, O. N. Mryasov, T. J. Klemmer and R. W. Chantrell, "Equilibrium Monte Carlo Simulations of A1-$L1_0$ Ordering in FePt Nanoparticles", *Scripta Materialia*, **53**, 417 (2005).

113. R. V. Chepulskii and W. H. Butler, "Temperature and Particle-Size Dependence of the Equilibrium Order Parameter of FePt Alloys", *Physical Review Letters B*, **72**, 134205 (2005).

114. Z. X. Tang, C. M. Sorensen and K. J. Klabunde, "Size-Dependent Curie Temperature in Nanoscale $MnFe_2O_4$ Particles", *Physical Review Letters*, **67**, 3602 (1991).

115. R. A. Ristau, K. Barmak, L. H. Lewis, K. R. Coffey and J. K. Howard, "On the Relationship of High Coercivity and $L1_0$ Ordered Phase in CoPt and FePt Thin Films", *Journal of Applied Physics*, **86**, 4527 (1999).

116. A. Hernando, I. Navarro, C. Prados, D. García, M. Vázquez and J. Alonso, "Curie-Temperature Enhancement of Ferromagnetic Phases in Nanoscale Heterogeneous Systems", *Physical Review B*, **53**, 8223 (1996).

117. T. B. Massalski, J. L. Murray, L. H. Bernet and H. Baker, "Binary Phase Diagrams", ASM International, Materials Park, Ohio, 1096 (1986).

118. H. N. Bertram, H. Zhou, and R. Gustafson, “Signal to noise ratio scaling and density limit estimates in longitudinal magnetic recording”, *IEEE Transactions on Magnetics*, **34**, 1845 (1998).

119. S. H. Charap, P. L. Lu, and Y. He, “Thermal stability of recorded information at high densities”, *IEEE Transactions on Magnetics*, **33**, 978 (1997).

120. D. Weller and A. Moser, “Thermal effect limits in ultrahigh density magnetic recording”, *IEEE Transactions on Magnetics*, **35**, 4423 (1999).

121. M. Watanabe, T. Nakayama, K. Watanabe, T. Hirayama, and A. Tonomura, “Microstructure and Magnetic Properties of High-Coercive Fe-Pt Alloy Thin Films”, *Materials Transactions*, *JIM*, **37**, 489 (1996).

122. Y. H. Wang, Y. Zhang, G. C. Hadjipanayis and D. Weller, “Fabrication and Characterization of Ordered FePt Nanoparticles”, *Journal of Applied Physics*, **93**, 7172 (2003).

123. W. F. Brown Jr., “Relaxational Behavior of Fine Magnetic Particles”, *Journal of Applied Physics*, **30**, S130 (1959).

BIOGRAPHICAL INFORMATION

Daren Li was born in Guangzhou, China. After graduating from high school, the author received higher education in the Department of Physics of Sun Yet-Sen University (Zhongshan University) and completed his Bachelor's Degree of Science in Physics there. After the graduation from college, the author felt the need of a better understating and broader knowledge of physics, which motivated him to continue graduate education in physics. He was admitted into the Department of Physics in the University of Texas at Arlington (UTA), Texas, USA, in 2002 and received his Master's Degree of Science in Physics in May 2006. In the author's master program, he worked as the main researcher in the project of Preparation and Characterization of Hard Magnetic Nanoparticles under the supervising of Dr. J. Ping Liu. Through working in this project, he has enriched his knowledge and experience in the area of Nano-Magnetism and Nanotechnology, which has drawn a great attention from all over the world. The work that he got involved in the development of advanced magnetic nano-materials (magnetic nanoparticles) was reported in the Physics Web for its significant contributions to the relevant research fields. Mr. Li is exploring more in the area of Materials Physics, as he will continue to pursue his Doctoral Degree in Physics.